



<https://doi.org/10.15407/ufm.24.02.319>

L. ROPYAK^{1,*}, T. SHIHAB^{1,2,}, A. VELYCHKOVYCH^{1,***},
O. DUBEI¹, T. TUTKO¹, and V. BILINSKYI¹**

¹ Ivano-Frankivsk National Technical University of Oil and Gas,
15 Karpatska Str., UA-76019 Ivano-Frankivsk, Ukraine

² Technical College of Engineering, Al-Bayan University,
International Airport Road, Near of Abbas Bin Firnas Sq.,
10070 Baghdad/Jadriya, Iraq

* liubomyr.ropiak@nung.edu.ua, l_ropjak@ukr.net,

** thaer.a@albayan.edu.iq, *** a_velychkovych@ukr.net

DESIGN OF A TWO-LAYER Al–Al₂O₃ COATING WITH AN OXIDE LAYER FORMED BY THE PLASMA ELECTROLYTIC OXIDATION OF Al FOR THE CORROSION AND WEAR PROTECTIONS OF STEEL

The article analyses technologies for the formation of coatings to protect machine and equipment parts from corrosion and wear in aggressive environments. The study considers plasma electrolytic oxidation (PEO) regimes of valve metal materials on the core, microstructure, and physical and mechanical properties of oxide coatings. To solve this problem, it is promising to develop a combined technology: application of a layer of aluminium on the surface of steel parts followed by its PEO. The purpose of this work is a theoretical study of the temperature distribution in a steel cylinder covered with a layer of aluminium during PEO to substantiate the thickness of the layers of the two-layer aluminium–aluminium oxide coating. An installation for PEO and a technological process of forming a two-layer Al–Al₂O₃ coating on long-dimensional parts are developed. A mathematical model is created for an infinite three-layer cylinder with an internal coaxial surface cylindrical source of

Citation: L. Ropyak, T. Shihab, A. Velychkovych, O. Dubei, T. Tutko, and V. Bilinskyi, Design of a Two-Layer Al–Al₂O₃ Coating with an Oxide Layer Formed by the Plasma Electrolytic Oxidation of Al for the Corrosion and Wear Protections of Steel, *Progress in Physics of Metals*, **24**, No. 2: 319–365 (2023)

© Publisher PH “Akadempriodyka” of the NAS of Ukraine, 2023. This is an open access article under the CC BY-ND license (<https://creativecommons.org/licenses/by-nd/4.0/>)

heat that moves at a constant speed in the radial direction deep into the aluminium layer of the cylinder. It is based on solving the boundary value problem of thermal conductivity with the condition of ideal thermal contact between the layers. During PEO, a solid oxide layer is formed, but the thickness of the unoxidized aluminium layer decreases. The thermophysical characteristics of such a cylinder are functions of both the radial co-ordinate of the cylinder and the time. During the construction of a two-layer coating, it is advisable to use the results of thermal calculations to justify the thickness of the unoxidized aluminium layer adjacent to the surface of the steel under the condition of ensuring the flow of mutual diffusion processes at the interface between aluminium and steel to increase the adhesion strength of the coating to the base due to heating by instantaneous heat sources caused by the action of electric-spark discharges in the PEO process. The thickness of the outer solid layer of aluminium oxide is chosen based on the condition of ensuring the necessary service life of machine parts for wear with a certain reservation. The results of mechanical, tribological, and corrosive cracking tests for steel samples with the developed two-layer Al_2O_3 coating show its high operational properties.

Keywords: two-layer coating, aluminium, aluminium oxide, steel, mathematical model, temperature, diffusion.

1. Introduction

The modern development of industry, transport, and population growth have led to a significant increase in the world's demand for energy, which is mainly met by various types of fossil hydrocarbon fuels, such as oil, gas, and coal [1]. Research results [2] show that energy security is an integral component of the national security system. According to the forecast of the International Energy Agency, liquid, gaseous and solid fuels of various types will occupy a significant place in the world energy balance by 2050 [3] despite the active development of alternative energy sources in recent years. Therefore, there is a need to develop oil and gas and coal deposits. Today, the urgent problem of the energy industry is the development of new innovative technologies [4–7] and tools [8–11], including taking into account the power load [12, 13], to increase the productivity of oil and gas deposits [14–16] and transportation of hydrocarbons [17], as well as the development of non-classical technological schemes for coal mining [18–20]. Successful implementation of the proposed innovations in practice requires the use of structural elements with special operational characteristics, which can be provided with the help of functionally modified and functionally gradient materials.

It should be noted that the development of new and the operation of existing oil and gas fields, which products contains corrosive components (hydrogen sulphide, carbon dioxide and others) and hard abrasive rock particles, impose increased demands on the quality of the surface layers of parts of geological exploration, drilling, oil and gas exploration and oil and gas transportation. Equipment is operated under static

and dynamic loads at high mechanical loads and elevated temperatures. The use of conventional structural carbon and alloy steels for the manufacture of parts of equipment and machines that operate in hydrogen sulphide environments and are subject to abrasive and hydroabrasive wear is not effective, since intensive hydrogen diffusion into steel occurs in such working conditions, which is especially dangerous for hardened steels, which leads to their hydrogen embrittlement [21–24]. Hydrogen has a small atomic radius, so it easily diffuses deep into the metal, where its atoms joint into molecules in voids (a hydrogen molecule is larger than atoms). It leads to tensile stresses and causes hydrogen embrittlement of hardened steels. To prevent corrosion cracking of carbon steels, their hardness is reduced, which in turn leads to a sharp decrease in wear resistance. Aluminium alloys are more resistant to hydrogen embrittlement, but have low hardness. Abrasive rock particles in many cases have a higher hardness than aluminium or steel parts. Therefore, there is a need to find new structural materials and technological methods of strengthening machine parts and equipment elements with coatings that would provide simultaneous protection against both hydrogen sulphide cracking and wear [25, 26]. Therefore, one of the effective methods of protecting steels from destruction is the application of various coatings.

High corrosion resistance in neutral, slightly acidic and slightly alkaline environments and a relatively high ratio between strength characteristics and specific weight are among the most important properties of aluminium alloys, which allow them to be used in various industries [27–29]. At the same time, such alloys are well processed by cutting and plastic deformation, have high electrical and thermal conductivity, good reflectivity and very good characteristics regarding reuse [30, 31]. These characteristics make aluminium alloys and composites very attractive and competitive structural materials for drill pipes [32]. However, the low wear resistance of aluminium alloys prevents their even wider application [33].

Today, there are a number of processing methods that are used to modify the surface of aluminium alloys [34–38], hard anodizing [39], electrochemical chrome plating [40], electrospark deposition, electric-spark alloying with various elements [41, 42], ion-plasma deposition [43] and high-speed oxygen-fuel HVOF coating [44]. Among the strengthening methods listed, plasma electrolytic oxidation (PEO) stands out favourably, which develops intensively and allows the formation of oxide coatings in the electrolyte on aluminium and metals of the valve group and their alloys [45–51], as well as directly on steel [52, 53] and other non-valve metals [54].

It should be noted that galvanic chrome coatings are the most frequently used among metal coatings, and oxide coatings are among non-

metallic ones. Therefore, PEO technology in many cases can be a cost-effective and environmentally safe alternative to galvanic chrome plating both for strengthening aluminium [40] and steel parts [55–59].

Ceramic coatings can significantly improve the surface properties of metal materials and provide excellent performance characteristics of products [45–60]. It should be noted the significant success of using PEO coatings to improve the properties of orthopaedic and dental implants [61–63].

The possibility to manage the metal alloy structure evolution, and phase transformations, formation under the influence of external factors has exceptional importance for metallurgical specialists to obtain the specified operational properties of the machine part surface layers to solve specific applied problems. The PEO regime change influence on microstructure and physical and mechanical properties of oxide coatings are of particular interest. The phenomenon that accompanies the PEO process of valve metals is a radical change in the thermophysical, mechanical, and dielectric properties of the surface layers. It is interesting that the growth kinetics of PEO coatings shows a close to linear dependence of the thickness on the oxidation time. At the same time, the rate of formation of oxide coatings is different for different metals.

Design and technological methods are usually used to ensure the reliable operation of machines whose parts are reinforced with coatings.

When designing coatings, a rational selection of materials [64], components of the composition taking into account their electrochemical properties of the elements [65–67], predictions of wear of coatings [68] and wear tests are carried out [69–71], mechanical properties are studied properties of coatings [72, 73], assess the level of residual stresses [74], model layered coatings [75], study the stress state of parts with coatings [76, 77] and study the temperature distribution in coatings [78–81].

Examples of successful assessment of the load-bearing capacity of compositions based on two criteria of strength (both coating and substrate) are studies of the equilibrium of layered ceramic-aluminium, the oxide layer of which is formed by PEO [82, 83], and SiO–Si [84, 85] coatings under local load, as well as studies of the limit state of cracked shells reinforced with a flexible coating [86–88].

Some analytical and analytical-numerical approaches to stress analysis in composite cylindrical bodies are considered in works [89–91]. The original method of studying temperature fields and stresses in layered structures of canonical form, which is based on the concept of quasi-derivative, was proposed in Refs. [92–94]. The phenomenon of temperature stress concentration near subsurface inclusions is described in articles [95, 96].

Technological methods include the selection of rational routes of mechanical wear [97], modes of mechanical processing to reduce manu-

facturing errors [98, 99], optimization technological parameters during manufacturing of the parts [100], including taking into account technological heredity [101–103], modes of forming oxide coatings [104–107], quality control of coatings [108–110] to ensure the operability of products with coatings during the life cycle [111, 112].

To form the protective coatings on parts made of aluminium and its alloys, as well as of metals of the valve group and their alloys, PEO is applied in the electrolyte. The applied high voltage between the part and the electrode, usually made of stainless steel, causes an electrical breakdown of the oxide film as well as the occurrence of sparks and micro-arc discharges on the surface of the part, which randomly migrate over the entire surface to be strengthened and lead to heating of the part and the electrolyte. Due to the course of plasma-chemical reactions in the discharge channels at high temperatures, dispersed oxides are formed that contain various phases, including α -Al₂O₃, providing the coating with high hardness and wear resistance [41–44, 50, 53, 71, 77, 113]. Since oxides are formed during PEO from the chemical elements of the alloy of the part and the electrolyte, the resulting coatings have a reliable (metallurgical, chemical) connection with the base. For accurate modelling of the nature of heat propagation from concentrated energy sources in multiphase composites and coatings [114], the necessary thermophysical properties of individual phases can be obtained based on statistical-thermodynamic calculations [115–117] and crystal-structure modelling from first principles calculations [118, 119].

The morphology of the resulting PEO coating is characterized by the ‘bubble’ structure. It indicates the modification of the metal surface, mainly by the mechanism of exothermic oxidation due to the flow of plasma-chemical reactions in which the components of the alloy and the electrolyte take part. During PEO, aluminium oxide is ejected from the discharge channel and crystallizes. This causes significant structural heterogeneity in the thickness of the oxide coating, which affects its hardness and mechanical properties. Under non-equilibrium conditions of heating and cooling in the PEO process, structural transformations occur and the formation of a surface oxide layer firmly connected to the aluminium base, which has a fundamentally different structure compared to that obtained during the use of traditional thermal, mechanical and electrochemical methods of forming oxide coatings. Usually, rapid hardening of the coating occurs in local areas of action of electrical discharges during PEO. Several features, including a very fine-grained structure and the presence of metastable phases, characterize this rapid process. It was established that in the oxide coating formed by PEO on aluminium alloy, in addition to the stable α -phase, there are γ -, η -, ε -phases of Al₂O₃ and several amorphous phases [47].

The formation of oxide coatings on steel and other structural materials without valve properties is carried out by PEO using special aluminate or silicate electrolytes [52]. Such measures do not always give the desired effect regarding the thickness, quality and protective properties of the oxide coating. Another approach is that a layer of metal with valve properties, for example, aluminium, is first applied to the working surface of the part, and then it is treated with PEO [45].

Aluminium [120] or aluminium alloys, for example, of the Al–Cu–Mg system [121], are preferably used to apply a metal layer to the surface of the part, which is subsequently subjected to PEO. During the strengthening of the titanium alloy, researchers [122] suggested that, in the process of applying a layer of aluminium by cold sputtering, it should be additionally reinforced with aluminium oxide particles before applying PEO, in order to increase the wear resistance of the oxide coating [123, 124]. The authors of the article [125] studied the processes of PEO applied to the surface of an aluminium alloy with a layer of aluminium with electroarc-sprayed, as well as a layer of aluminium with the inclusion of Cu and Ni with the plasma spraying. The work [126] investigated the effect of magnetron sputtering of aluminium layer and PEO on the corrosion and wear resistances of AZ31 magnesium alloy and established a significant increase in corrosion resistance and reduction of wear during dry friction.

Austenitic steel was successfully aluminized by pack aluminizing and hot-dip aluminizing processes and treated with PEO to increase heat-resistance [127]. During the study of the PEO process on hot dip aluminized cast iron with high phosphorus content [128], the influence of the duration of oxidation on the nature of the growth of the oxide layer of the coating, its phase composition, surface roughness, dimensional change, and tribological properties was determined.

The results of the study [129] indicate a high protective effect against corrosion in seawater and wear of a two-layer coating formed on steel by thermal spraying of an aluminium layer followed by its PEO modification. Works [130–132] studied the structure, investigated the corrosion resistance and wear resistance of oxide coatings on steel prepared of hot-dipping aluminium and PEO. The research results presented in Ref. [133] illustrate the possibility of applying such combined coatings to the inner surface of pipes. The results indicate that metallurgical bonding can be observed between the coatings and the steel substrate. It should be noted that this metallurgical connection occurs at the stage of hot aluminization of hot-dipping aluminium steel.

A number of studies are devoted to the study of PEO processes of aluminium layers applied to a steel base by various methods, in particular, of hot-dipping aluminium [134], electroarc-sprayed [135, 136], electroarc-spraying and flame spraying of Al coatings ($\text{Al}_{99.5}$ and AlCu_4Mg_1)

[137,138], and electrospark deposition [139]. That is, the PEO processes of aluminium layers pre-applied on a steel base and other alloys have been studied in sufficient detail. A layer of aluminium is applied to the steel base by any known method. The technology of forming by a combined method using PEO double-layer Al–Al₂O₃ coatings is a viable and attractive option for strengthening both during the manufacture of new and restoration of worn machine parts. It should be noted that it is quite difficult to apply a coating of valve metals to steel by the galvanic method. Thermal spraying methods, such as high-speed oxy-fuel spraying, plasma spraying, electric-arc spraying and detonation spraying, cladding, *etc.*, are widely used at present, but the common problem of coatings obtained in this way is insufficient reliability of the mechanical connection of the coating layer with the base [140–142]. During the practical application of protective coatings to strengthen machine parts, the problem of their premature destruction is often encountered, mainly due to peeling and cracking.

Abnormal conditions of operation of machines and equipment, exceeding the design operating loads can cause unintentional and accelerated loss of service life of elements with protective coatings. Therefore, the composition ‘base material–coating’ should always be required to combine a high level of special properties (for example, hardness, wear resistance, friction coefficient, corrosion resistance) with a sufficient margin of strength, reliability and durability. Here, first, the strength of the composition ‘base material–coating’ should be evaluated as a layered deformable body under the action of operational loads [77]. Resistance to destruction and performance during operation of both the coating itself and the element covered with the coating in general depend on their stress-deformed state and the strength of the adhesion of the coating to the base. At the same time, the effectiveness of the protective action of the layered coating, especially the anticorrosion protection against flooding in hydrogen sulphide environments of the oil and gas industry, depends significantly on the integrity and thickness of the coating, the strength of the adhesion of the layers to the steel base of the part.

It is widely recognized that the stability of the coating-substrate interface is related to the interfacial adhesion forces and electrochemical properties of this region. That is why great attention should be paid to the selection of rational thicknesses of coating layers to ensure both the strength of adhesion to the base and the necessary service life of machine parts during wear in aggressive corrosive environments.

In addition, in practice, there is a problem that it is difficult to choose the thickness of the remaining unoxidized layer of aluminium adjacent to the surface of the steel part during the PEO process. The results of our methodical experiments showed that in the case of applying PEO to the entire thickness of the pre-applied aluminium layer,

electrical breakdowns occur on the steel, which reduce the adhesion strength of the coating to the base, and in some cases, complete peeling of the coating may occur, which nullifies all the advantages of PEO, which consist in very good adhesion of aluminium oxide to the aluminium coating layer from which this oxide is actually formed. Therefore, it is advisable to turn the outer part of the aluminium layer into ceramic with PEO, and leave the inner part (sublayer) of aluminium adjacent to the steel surface unoxidized. However, a systematic study on the substantiation of the thicknesses of coating layers, which are formed by a combined method (applying a layer of aluminium on steel and using PEO), is practically absent, which prevents their rational design and use in production for strengthening machine parts and was not well documented in the patent and scientific and technical literature.

The purpose of this work is the theoretical substantiation of the thickness of the two-layer aluminium–aluminium oxide coating to ensure a reliable connection of the unoxidized aluminium coating layer with the steel base of the part during the implementation of the PEO process in the electrolyte and conducting mechanical and corrosion tests.

To achieve the goal, the following tasks should be solved:

- to improve the technology of formation by the combined method of two-layer Al–Al₂O₃ coatings on a steel base using PEO;
- to construct the mathematical model of temperature distribution during PEO of an aluminium coating layer applied to a cylindrical steel base;
- to determine the thickness of the unoxidized aluminium layer adjacent to the steel surface, at which mutual diffusion processes occur at the steel base–aluminium interface under the action of instantaneous heat sources caused by the occurrence of spark discharges during PEO of the outer part of the aluminium coating layer in the electrolyte;
- to study mechanical, tribological and corrosion properties of Al–Al₂O₃ coatings.

2. Materials and Methods

2.1. Materials and Technology for the Formation of a Two-Layer Al–Al₂O₃ Coating

Figure 1 shows the scheme of the developed combined technology using PEO for the formation of a two-layer coating of Al–Al₂O₃ on steel parts, which includes a number of operations: applying a layer of aluminium to the steel workpiece by any known method; conducting PEO while leaving the aluminium layer adjacent to the steel surface unoxidized; carrying out mechanical processing (if necessary); preparation of the surface of the part before applying the aluminium layer is carried out

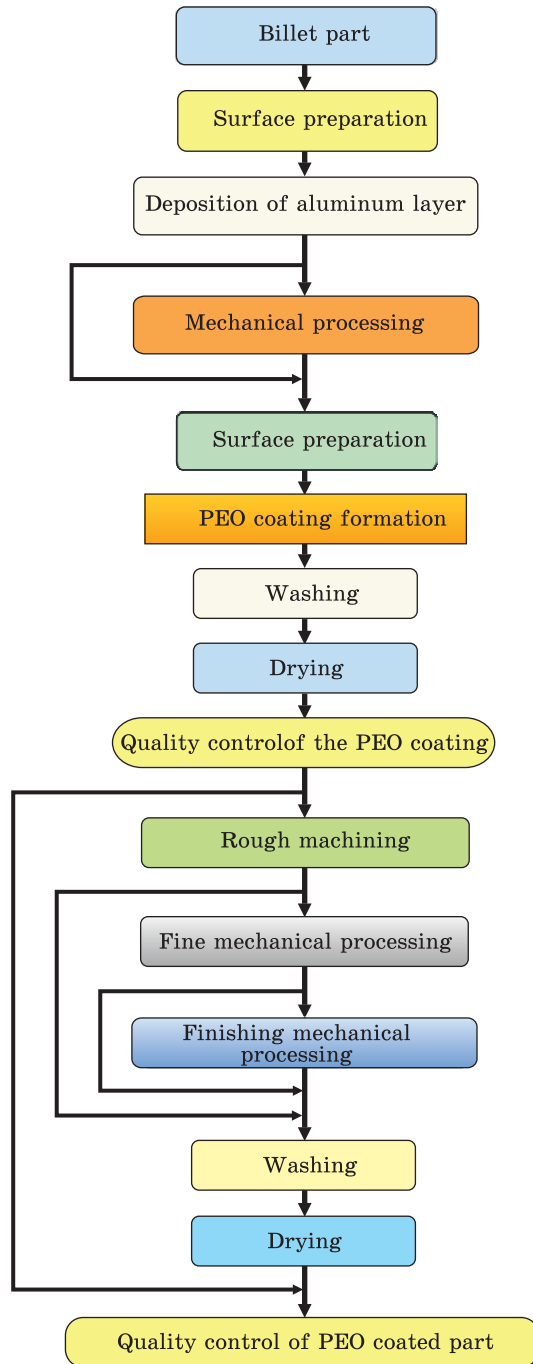
Fig. 1. Structural diagram of the technological process of forming on steel by a combined method using PEO double-layer coating Al–Al₂O₃

by common methods; washing of parts after PEO is usually carried out in water.

Blanks of cylindrical parts were made from high-quality structural carbon steel 45 State Standard GOST 1050–2013 (analogues of European Union 1.1191, 2C45, C45, C45E, C45EC, C46). The heat treatment of carbon steel 45 samples was as follows: quenching from 850 °C in water and tempering at a temperature of 460 °C. The resulting mechanical properties were the yield strength $\sigma_{0.2} = 1100$ MPa and the hardness of 34 HRC. Chemical composition of the steel 45 and properties of the steel 45, aluminium and aluminium oxide are presented in Table 1 and Table 2, respectively.

The electric arc spraying of the aluminium coating layer on the steel cylindrical workpiece was carried out on a research and industrial installation constructed by us on the basis of a modernized electrometallization apparatus ED-6, installed on the support of a TV-16 lathe, equipped with a three-jaw chuck and a rotating rear centre.

The PSG-500 welding converter served as the source of electric current for the ED-6 device, and the current was regulated by the RB-301 bal-



last rheostat. The SO-7A compressor, equipped with a receiver and an oil separator, provided compressed air through a nozzle for metal spraying of two aluminium wires melted by an electric arc on the surface of the workpiece. Modes (parameters) of electric arc spraying: aluminium wire diameter of 2 mm (State Standard GOST 7871–75), spraying distance of 100 mm, spraying air pressure of 610 kPa, voltage of 20–30 V, current of up to 100 A, aluminium layer thickness of 250–300 μm .

The PEO process of the aluminium layer of the coating applied to the steel cylindrical workpiece of the part was implemented on the installation developed by us, which contains a galvanic bath for the electrolyte, an electric stirrer, a process current source, and a water cooling system; a control system for technological parameters of the process (anode, cathode voltage, anode, cathode current and temperature), an exhaust ventilation system and a blocking system against electric shock. The galvanic bath is made of stainless steel 12Ch18N10T (State Standard GOST 563–72), is made in the form of a vertical cylindrical tank with two walls that form a jacket for water cooling, and is installed on electrically insulating supports in an extraction cabinet. The galvanic bath (counter electrode) and the cylindrical workpiece of the part (electrode), which is processed by PEO, are connected by appropriate current leads to the capacitor-type process current source, which is powered by industrial network (380 V, 50 Hz). During PEO, the workpiece is installed coaxially with the vertical axis of the galvanic bath; the fume hood is closed with a transparent curtain made of organic glass, which interacts with the limit switch of the blocking system, which makes it impossible to turn on the electrical power of the installation when the curtain is open. For the PEO of the aluminium coating layer, a silicate–alkaline electrolyte was used, which contained 2 g/l potassium hydroxide (KOH,

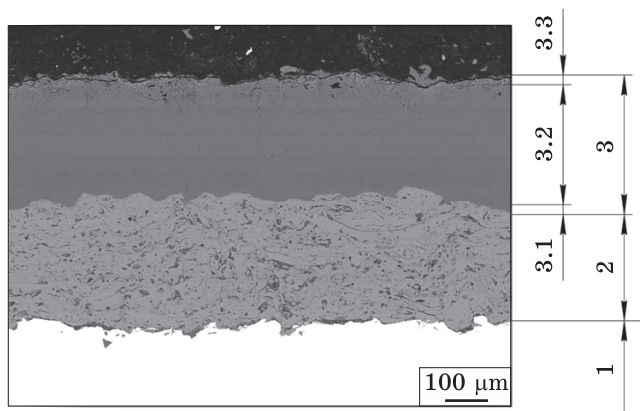
Table 1. Chemical composition of the carbon steel 45, mass.% (GOST 1050–2013)

C	Si	Mn	P	S	Cr	Ni	Cu	Fe
0.42–0.50	0.17–0.37	0.50–0.80	0.030	0.035	0.25	0.30	0.30	The rest

Table 2. Physical and mechanical properties of carbon steel 45, aluminium and aluminium oxide

Material	$\sigma_{0.2}$, MPa	HB, GPa	E, GPa	T_m , °C	$\alpha \cdot 10^5$, deg ⁻¹ [160]	λ , W/(m·deg) [159]	ρ , kg/m ³ [159]	C, J/(kg·deg) [45, 160]
Steel 45	1100	3.11	200	1450	1.19	38	7826	473
Aluminium	67	1	72	659	2.29	209	2680	920
Aluminium oxide	300	22	247	2072	0.782	21.3	3950	0.905

Fig. 2. Cross-sectional morphology of two-layer coating Al–Al₂O₃ on carbon steel 45: 1 — steel, 2 — a unoxidized layer of aluminium, 3 — layer of aluminium oxide formed by PEO; 3.1 — transition layer, 3.2 — functional layer, 3.3 — porous layer



State Standard GOST 9285-78) and 9 g/l sodium silicate (Na₂SiO₃, State Standard GOST 13078-81), dissolved in distilled water. The electrolyte was prepared from chemically pure components by simply mixing them in distilled water, which was obtained using a water distiller DE-4-2. PEO process modes: current density of 5 A/dm², voltage of up to 760 V, electrolyte temperature of 65–70 °C, thickness of the oxide coating layer of 125–250 μm.

The thickness of the coating layers was determined on transverse microsections using a PMT-3 hardness tester using an eyepiece micrometre with a resolution of 1 μm. We conducted the microscopic studies of coatings Al–Al₂O₃ formed on carbon steel 45 at the Centre for collective use of scientific instruments ‘Centre for Electron Microscopy and X-Ray Microanalysis’ of the Karpenko Physico-Mechanical Institute of the National Academy of Sciences of Ukraine (Lviv). We used a ZEISS EVO 40XVP scanning electron microscope (adjusted in the electron backscatter diffraction (BSD) mode) (ZEISS Group, Jena, Germany).

A typical structure of a two-layer coating on steel is presented in Fig. 2. Porous layer 3.3 is usually removed by mechanical processing. In the two-layer Al–Al₂O₃ coating, the outer oxide layer is the working layer and consists of the transition layer 3.1 and the functional layer 3.2, and the inner unoxidized aluminium layer 2 ensures a reliable connection of the working oxide layer with the steel base 1. Sometimes this layer of aluminium 2 can act as a barrier, for example, to protect the steel base 1 from hydrogen penetration during the operation of coated machine parts in aggressive corrosive environments containing hydrogen sulphide.

During the construction of the two-layer Al–Al₂O₃ coating, it is proposed to choose rationally the thicknesses of the layers based on the following considerations. The thickness of the solid-oxide working layer should be chosen from the condition of ensuring the necessary service

life of the wear parts of the machines with a certain reserve. Since the corrosion rate of this oxide layer is quite low in most production environments, it can be neglected. The thickness is calculated according to known formulas based on the results of laboratory and industrial tests of oxide coatings for wear, taking into account abrasive environments and operational loads.

A hypothesis was put forward about the possibility of choosing the thickness of the unoxidized layer of aluminium adjacent to the steel under the condition of ensuring the flow of mutual diffusion processes between aluminium and steel due to the action of instantaneous heat sources, the occurrence of which is caused by electric spark discharges during the breakdown of the oxide layer in the PEO process of aluminium. This approach will increase the bond strength of the layered coating with the steel base.

2.2. Mechanical, Tribological and Stress Corrosion Cracking Testing

The authors determined the steel base–coating adhesion strength by the adhesive method. The coating was formed on the end surface of steel cylindrical samples with a length of 10 mm and a diameter of 10 mm. For testing, the coated sample was glued coaxially to a similar steel counter-sample without coating with VK-31 glue. Glue polymerization was carried out under a load of 1 MPa at a temperature of 175 °C for 90 min in an electric resistance furnace. Detachment of the coating from the surface of steel cylindrical samples with a diameter of 10 mm was carried out on an ‘Instron’ tearing machine using self-centring grippers. The adhesion strength of the coating to the steel base was calculated using the formula $\sigma = 4F/\pi d^2$, where F is the pull-off force; π is a constant number ($\cong 3.14$); d is the diameter of the cylindrical sample with a coating on the end, $d = 10$ mm. The value of the adhesion strength of the coating to the steel base was determined as the arithmetic mean of the results of five test samples.

Laboratory testing of steel specimens with coatings for resistance to sulphide stress cracking and stress corrosion cracking in H₂S environments has been performed in accordance with the recommendations of NACE Standard TM01772005, Item No. 21212. The test solution is an acidified and buffered, H₂S saturated aqueous brine solution: consist of 5.0 wt.% NaCl and 0.5 wt.% CH₃COOH dissolved of distilled water, H₂S saturation (2.5–3.0 g/l), pH 2.6–2.8 for testing at room temperature and atmospheric pressure. During the test, the pH did not exceed 4.0. Cylindrical steel specimens with a working part diameter of 3.81 ± 0.05 mm and a height of 15 mm were used for uniaxial tensile tests, both with and without coatings. The non-working part of the samples was covered with varnish. The samples were loaded on a self-

made lever system. Steel samples with a single-layer Al coating with a thickness of 250 μm and a two-layer Al–Al₂O₃ coating with a total thickness of 250 μm were tested with different thicknesses of the unoxidized Al layer: 125 μm ; 65 μm ; 35 μm . Samples of heat-treated carbon steel 45 without coating were used as the etalon. The highest no-failure stress in was determined after 720 hours of testing. The static strength value (the maximum stress, at which the steel samples in the test solution do not break during the base time of 720 hours) was determined as the arithmetic mean of the results of three tests of the samples.

To carry out tribological studies, a machine was used for testing samples with wear coatings according to the cylinder-disc scheme under conditions of dry sliding friction. The test specimens had the shape of a cylinder with a diameter of 3 mm and a height of 20 mm with a two-layer Al–Al₂O₃ coating on the end. The samples were mounted on a holder and slid with an oxide coating on the flat end face of a carbon steel grade 45 disk with hardness of 34 HRC in a reciprocating motion in the radial direction to the axis of rotation of the disk/periphery of the disk. Steel samples without coating served as the standard. The specific load of the sample and the average sliding speed were of 30 MPa and 0.3 m/min, respectively. The friction path of the sample along the Archimedean spiral was of 5000 m. The wear of the samples was measured using a watch-type indicator with a division accuracy of 1 μm for three samples.

2.3. Mathematical Model of Al–Al₂O₃ Two-Layer Coating

2.3.1. Physical Formulation of the Problem

The authors consider a cylindrical body with a length providing practically independence of its value in the middle part from axial coordinate of the cylinder during body's temperature field determination caused by heat sources of equal power along the axis. In terms of the mathematical formulation of the problem, an infinite cylinder can replace by a finite one.

The steel cylinder with the radius of r_1 is pre-coated with a thick layer of aluminium with the thickness of h . The outer diameter of the cylinder is $d_2 = 2(r_1 + h)$. Then, the PEO process is implemented in the electrolyte, because of which the outer part of the aluminium layer is transformed into aluminium oxide, but at the same time, the total thickness of the formed aluminium oxide layer and the unoxidized aluminium layer remains unchanged. This means that during the PEO of parts, the thickness of the Al₂O₃ oxide layer increases and the thickness of the Al layer, on the contrary, decreases.

During PEO, because of the occurrence of spark and microarc discharges, which pierce the oxide film on the outer surface of the aluminium layer, plasma-chemical and electrochemical reactions occur. The

main products of these reactions are aluminium oxides. The heat released during discharges causes an increase in temperature in the oxide layer, the unoxidized layer of aluminium and the steel base (cylinder), as well as heating of the electrolyte.

Let us assume that spark discharges occur at the aluminium–aluminium oxide interface and are point discharges. Due to the uniformity of the aluminium oxide layer formation and difficulty to specify the spark discharge distribution regularity on the outer surface of the cylinder to study the temperature field in such a system, we will replace the total spark discharges (their thermal power) with a surface (cylindrical) heat source that takes place on the boundary aluminium oxide–unoxidized aluminium. The power of this heat source over the entire surface of the cylinder is assumed to be constant [W/m^2], and its total power is equal to the total thermal power of the spark discharges. Since the thickness of the oxide layer increases in the PEO process, this means that the heat source moves into the depth of the cylinder in the radial direction.

The surface of the cylinder is washed with electrolyte in a galvanic bath, which is cooled by running water at a constant temperature. Thus, the temperature on the surface of the cylinder can be considered constant and equal to the temperature of the electrolyte (boundary condition of the first kind).

From the point of view of the theory of heat conduction, we have a temperature problem for a three-layer cylinder with an internal coaxial surface cylindrical heat source that moves at a constant speed in the radial direction deep into the aluminium layer of the cylinder. At the same time, the thickness of the upper formed layer of the cylinder (aluminium oxide) increases, but the thickness of the second layer (unoxidized aluminium layer) decreases. The thermophysical characteristics of such a cylinder are functions of both the co-ordinates within the cylinder and the time. Therefore, the one-dimensional problem is non-stationary.

2.3.2. Derivation of the Differential Equation for a Three-Layer Cylinder with a Moving Boundary between the 2nd and 3rd Layers and a Heat Source between Them

We have a three-layer cylinder (Fig. 3). The thermophysical properties of each layer in this case are functions of the intracylinder co-ordinate r . They can be represented by the following expressions [143]:

$$\begin{aligned} \lambda_t(r, \tau) &= \lambda_t^{(1)} + (\lambda_t^{(2)} - \lambda_t^{(1)})S_-(r - r_1) + (\lambda_t^{(3)} - \lambda_t^{(2)})S_-(r - r_1 + (h - v\tau)), \\ c(r, \tau) &= c^{(1)} + (c^{(2)} - c^{(1)})S_-(r - r_1) + (c^{(3)} - c^{(2)})S_-(r - (r_1 + h - v\tau)), \\ \rho(r, \tau) &= \rho^{(1)} + (\rho^{(2)} - \rho^{(1)})S_-(r - r_1) + (\rho^{(3)} - \rho^{(2)})S_-(r - (r_1 + h - v\tau)), \end{aligned} \quad (1)$$

where r , τ are the radial co-ordinate within the cylinder and the time

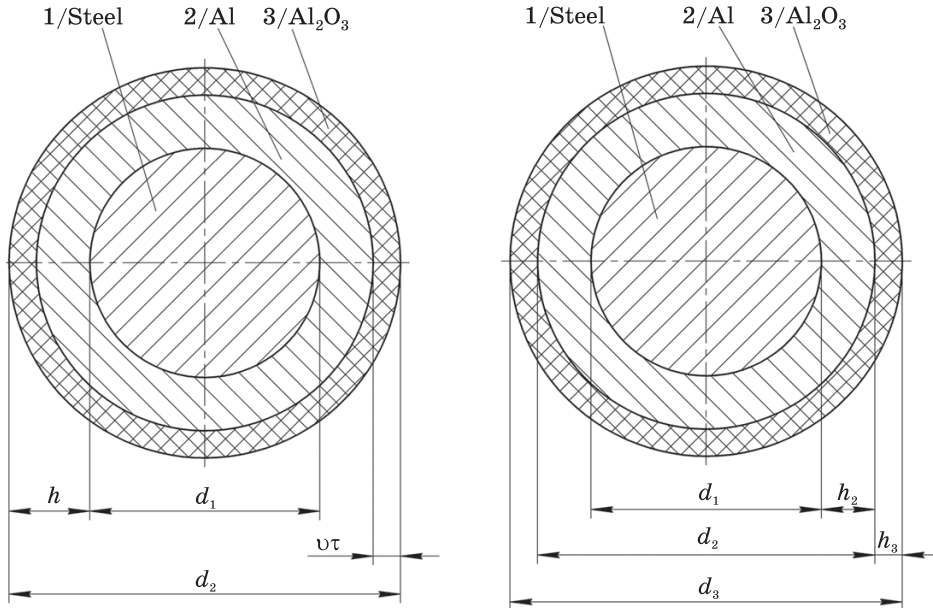


Fig. 3. Calculation scheme of the three-layer cylinder

Fig. 4. Calculation scheme of the three-layer cylinder (redefinition of dimensions)

from the PEO process starting; λ_t , r , $c(r, \tau)$, $\rho(r, \tau)$ are coefficient of thermal conductivity, specific heat capacity and density of the material at arbitrary points of the cylinder, respectively; $\lambda_t^{(1)}$, $\lambda_t^{(2)}$, $\lambda_t^{(3)}$ are thermal conductivity coefficients of the 1st, 2nd, and 3rd layers, respectively; $c^{(1)}$, $c^{(2)}$, $c^{(3)}$ are specific heat capacity of the 1st, 2nd, and 3rd layers, respectively; $\rho^{(1)}$, $\rho^{(2)}$, $\rho^{(3)}$ are material density of the 1st, 2nd and 3rd layers of the cylinder, respectively; $S_-(r - r_1)$, $S_-(r - (r_1 + h - v\tau))$ are asymmetric unit functions [144]:

$$S_-(x) = \begin{cases} 1, & x \geq 0, \\ 0, & x < 0; \end{cases}$$

v is aluminium-oxide layer thickness increasing rate, in other words, the rate of cylindrical heat-source displacement.

The heat conduction equation for a non-homogeneous cylinder has the form:

$$c\rho \frac{\partial T}{\partial \tau} = \frac{\partial \lambda_t}{\partial r} \frac{\partial T}{\partial r} + \frac{\lambda_t}{r} \frac{\partial T}{\partial r} + \lambda_t \frac{\partial^2 T}{\partial r^2} + w. \quad (2)$$

The source function w is written as

$$w = q\delta_-(r - (r_1 + h - v\tau)), \quad (3)$$

where q is the power of the surface (cylindrical) heat source [W/m²]; $\delta_-(r - (r_1 + h - v\tau))$ is asymmetric delta function [144]:

$$\delta_-(r - (r_1 + h - v\tau)) = \frac{\partial S_-(r - (r_1 + h - v\tau))}{\partial r}.$$

Let us find the derivative $\partial\lambda_t/\partial r$:

$$\frac{\partial\lambda_t}{\partial r} = (\lambda_t^{(2)} - \lambda_t^{(1)})\delta_-(r - r_1) + (\lambda_t^{(3)} - \lambda_t^{(2)})\delta_-(r - (r_1 + h - v\tau)). \quad (4)$$

It can be shown that

$$c(r, \tau)\rho(r, \tau) = c^{(1)}\rho^{(1)} + (c^{(2)}\rho^{(2)} - c^{(1)}\rho^{(1)})S_-(r - r_1) + (c^{(3)}\rho^{(3)} - c^{(2)}\rho^{(2)})S_-(r - (r_1 + h - v\tau)) \quad (5)$$

Let us substitute Eqs. (3)–(5) and the first formula of the system of expressions (1) into Eq. (2):

$$\begin{aligned} & \left[c^{(1)}\rho^{(1)} + (c^{(2)}\rho^{(2)} - c^{(1)}\rho^{(1)})S_-(r - r_1) + \right. \\ & \left. + (c^{(3)}\rho^{(3)} - c^{(2)}\rho^{(2)})S_-(r - (r_1 + h - v\tau)) \right] \frac{\partial T}{\partial \tau} = \\ & = \left[(\lambda_t^{(2)} - \lambda_t^{(1)})\delta_-(r - r_1) + (\lambda_t^{(3)} - \lambda_t^{(2)})\delta_-(r - (r_1 + h - v\tau)) \right] \frac{\partial T}{\partial r} + \quad (6) \\ & + \left(\frac{\partial^2 T}{\partial r^2} + \frac{1}{r} \frac{\partial T}{\partial r} \right) \left[\lambda_t^{(1)} + (\lambda_t^{(2)} - \lambda_t^{(1)})S_-(r - r_1) + \right. \\ & \left. + (\lambda_t^{(3)} - \lambda_t^{(2)})S_-(r - (r_1 + h - v\tau)) \right] + q\delta_-(r - (r_1 + h - v\tau)). \end{aligned}$$

We divide the left and right parts of Eq. (6) by

$$\left[\lambda_t^{(1)} + (\lambda_t^{(2)} - \lambda_t^{(1)})S_-(r - r_1) + (\lambda_t^{(3)} - \lambda_t^{(2)})S_-(r - (r_1 + h - v\tau)) \right],$$

and, at the same time, we obtain the differential equation of thermal conductivity for a three-layer cylinder in the following form:

$$\begin{aligned} \frac{\partial^2 T}{\partial r^2} + \frac{1}{r} \frac{\partial T}{\partial r} &= \left[\frac{1}{a_1} + \sum_{i=1}^2 \left(\frac{1}{a_{i+1}} - \frac{1}{a_i} \right) S_-(r - r_i) \right] \frac{\partial T}{\partial \tau} + \\ &+ \sum_{i=1}^2 \left(1 - \frac{\lambda_t^{(i+1)}}{\lambda_t^{(i)}} \right) \delta_-(r - r_i) \frac{\partial T}{\partial r} \Big|_{r=r_i} - \quad (7) \\ &- \left[\frac{1}{\lambda_t^{(1)}} + \sum_{i=1}^2 \left(\frac{1}{\lambda_t^{(i+1)}} - \frac{1}{\lambda_t^{(i)}} \right) S_-(r - r_i) \right] q\delta_-(r - r_2), \end{aligned}$$

where $r_2 = r_1 + h - v\tau$; a_i is the coefficient of thermal conductivity of the i -th layer of the cylinder.

Considering $S_-(r - r_2)\delta_-(r - r_2) = 0$ [143], Eq. (7) takes the following final form:

$$\begin{aligned} \frac{\partial^2 T}{\partial r^2} + \frac{1}{r} \frac{\partial T}{\partial r} &= \left[\frac{1}{a_1} + \sum_{i=1}^2 \left(\frac{1}{a_{i+1}} - \frac{1}{a_i} \right) S_-(r - r_i) \right] \frac{\partial T}{\partial \tau} + \quad (8) \\ &+ \sum_{i=1}^2 \left(1 - \frac{\lambda_t^{(i+1)}}{\lambda_t^{(i)}} \right) \delta_-(r - r_i) \frac{\partial T}{\partial r} \Big|_{r=r_i} - \frac{q}{\lambda_t^{(2)}} \delta_-(r - r_2). \end{aligned}$$

If we include the initial and boundary conditions to the differential Eq. (8), then, we will have a boundary value problem for a three-layer cylinder. In our case, these conditions will be as follow:

$$T(r_1 + h, \tau) = T_c, \quad (9)$$

$$T(r, 0) = T_0, \quad (10)$$

where T_c is the temperature of the electrolyte on the surface of the cylinder $r = r_1 + h$; T_0 is the initial temperature of the points of the cylinder ($T_0 = \text{const}$).

The boundary value problem (8)–(10) is rather complicated. The first reason for the complexity is related to the fact that we are not considering a homogeneous cylinder, but a three-layer one, and the second reason, which causes the greatest complexity, is that over time the thickness of the second and third layers changes, although their total thickness remains the same. That is, we have a problem with a moving boundary between the second and third layers of the cylinder.

Heat conduction problems with moving boundaries belong, as indicated in Refs. [145, 146], to one of the most complex classes of non-stationary heat conduction problems. Therefore, the boundary value problem (8)–(10) requires a certain simplification to obtain an analytical solution. If we take into account the fact that the thickness of the 2nd and 3rd layers is extremely small compared to the radius of the cylinder r_1 , then, this means the possibility of replacing the variable thicknesses of the 2nd and 3rd layers with their average values when determining the temperature field in the cylinder of radius r_1 . We are primarily interested in the temperature field in the steel cylinder, on which the diffusion processes at the interface between the steel cylinder and the aluminium layer (unoxidized) depend.

Let the constant values of the thicknesses of the 2nd and 3rd layers be, respectively, h_2 and h_3 ; $h_2 + h_3 = h$ (Fig. 4). Then, we will make a substitution in Eq. (8): $r_2 = r_1 + h_2$.

Taking into account the simplification of the problem ($h_2 = \text{const}$, $h_3 = \text{const}$), two approaches to finding the solution of the boundary value problem (8)–(10) can be indicated. The first approach is to solve the differential heat-conduction Eq. (8) for a three-layer cylinder under the boundary conditions (9), (10). In the second approach, the insignificant thickness of the 2nd and 3rd layers can be taken into account, and this will allow obtaining the heat exchange condition at the boundary between the non-radiated layer of aluminium and the steel cylinder when using the operator method [147] and further determine the temperature field in the steel cylinder under the imposed boundary condition.

The use of the operator method to determine the heat exchange conditions at the edges of shells and plates reinforced with thin elements is known in the scientific literature [148–150]. Let us first

apply the second approach to determine the temperature field in a steel cylinder.

2.3.3. Heat Exchange Condition at the Interface between the Steel Cylinder and the Aluminium Layer

To obtain the heat exchange condition at the boundary between a steel cylinder and a layer of unoxidized aluminium, we first derive the differential equation of heat conduction for a two-layer hollow cylinder, which consists of an aluminium layer 2 and an aluminium-oxide layer 3.

We will use Eq. (2). The function $\lambda_t(r)$ in this case is characterized as follows:

$$\lambda_t(r) = \lambda_t^{(2)} + (\lambda_t^{(3)} - \lambda_t^{(2)})S_-(r - (r_1 + h_2)), \tag{11}$$

moreover, its derivative is

$$\frac{d\lambda_t}{dr} = (\lambda_t^{(3)} - \lambda_t^{(2)})\delta_-(r - (r_1 + h_2)). \tag{12}$$

Now the power of the internal heat source will be

$$w = q\delta_-(r - (r_1 + h_2)). \tag{13}$$

The product of the specific heat capacity and the density of the material of the hollow cylinder will have the form [143]:

$$c(r)\rho(r) = c^{(2)}\rho^{(2)} + (c^{(3)}\rho^{(3)} - c^{(2)}\rho^{(2)})S_-(r - (r_1 + h_2)). \tag{14}$$

We substitute Eqs. (11)–(14) in Eq. (2) and get:

$$\begin{aligned} & \left[c^{(2)}\rho^{(2)} + (c^{(3)}\rho^{(3)} - c^{(2)}\rho^{(2)})S_-(r - (r_1 + h_2)) \right] \frac{\partial T}{\partial \tau} = \\ & = (\lambda_t^{(3)} - \lambda_t^{(2)})\delta_-(r - (r_1 + h_2)) \frac{\partial T}{\partial r} \Big|_{r=r_1+h_2} + \\ & + \frac{1}{r} \left[\lambda_t^{(2)} + (\lambda_t^{(3)} - \lambda_t^{(2)})S_-(r - (r_1 + h_2)) \right] \frac{\partial T}{\partial r} + \\ & + \left[\lambda_t^{(2)} + (\lambda_t^{(3)} - \lambda_t^{(2)})S_-(r - (r_1 + h_2)) \right] \frac{\partial^2 T}{\partial r^2} + q\delta_-(r - (r_1 + h_2)). \end{aligned}$$

We divide the left and right parts of the last equation by $\lambda_t(r)$, and, as a result, we get the thermal conductivity equation for a two-layer hollow cylinder in the following form:

$$\begin{aligned} & \frac{\partial^2 T}{\partial r^2} + \frac{1}{r} \frac{\partial T}{\partial r} = \left[\frac{1}{a_2} + \left(\frac{1}{a_3} - \frac{1}{a_2} \right) S_-(r - (r_1 + h_2)) \right] \frac{\partial T}{\partial \tau} + \\ & + \left(\mathbf{1} - \frac{\lambda_t^{(3)}}{\lambda_t^{(2)}} \right) \delta_-(r - (r_1 + h_2)) \frac{\partial T}{\partial r} \Big|_{r=r_1+h_2} - \frac{q}{\lambda_t^{(2)}} \delta_-(r - (r_1 + h_2)). \end{aligned} \tag{15}$$

Equation (15) describes the temperature field in a two-layer hollow cylinder, that is, in contact with a cylinder whose radius is r_1 . Since the coating layers are very thin, we will try to replace the temperature field of a thin two-layer cylinder with a complicated boundary condition at the boundary of the second cylindrical layer–steel cylinder ($r = r_1$). At the same time, the system cylinder–two-layer hollow cylinder is referred to the curvilinear coordinate system [151] (s, n), where s means the distance along the boundary between the layers of the hollow cylinder from certain position $s = 0$; n is the distance from any point along the normal to the boundary line between the layers.

The boundary value problem of thermal conductivity for a two-layer cylinder will now be written as follows:

$$\Delta T^* - \left[\frac{1}{a_2} + \left(\frac{1}{a_3} - \frac{1}{a_2} \right) S_-(r - (r_1 + h_2)) \right] \frac{\partial T^*}{\partial \tau} =$$

$$= \left(1 - \frac{\lambda_t^{(3)}}{\lambda_t^{(2)}} \right) \delta_-(r - (r_1 + h_2)) \frac{\partial T^*}{\partial r} \Big|_{r=r_1+h_2} - q \frac{1}{\lambda_t^{(2)}} \delta_-(r - (r_1 + h_2)). \quad (16)$$

Initial condition ($\tau = 0$) is

$$T^* = T_0 \quad (T_0 = \text{const}); \quad (17)$$

conditions of ideal thermal contact with a steel cylinder ($n = -h_2$) is

$$T^* = T_0, \quad \lambda_t^{(2)} \frac{\partial T^*}{\partial n} = \lambda_t^{(1)} \frac{\partial T}{\partial n}; \quad (18)$$

in addition, the boundary condition ($n = h_3$) is

$$T^* = T_c, \quad (19)$$

where T_0, T_c are the initial temperature of the points of the cylinder and the temperature of the medium (electrolyte) washing the cylinder in the galvanic bath, respectively; T^* is the temperature of the points of a two-layer hollow cylinder (redesignated); T is the temperature of the points of the steel cylinder; Δ is the Laplace operator associated with the base surface for the axisymmetric problem.

Note that condition (18) can be considered as an equation with derivatives in the direction with respect to T or T^* . Then, its solution in the class of analytic functions will be functions of bounded index in the direction n [152, 153].

In the coordinate system (s, n), the Laplace operator has the form [151]:

$$\Delta = \left(\frac{1}{D} \right) \left\{ \frac{\partial}{\partial n} \left[D \frac{\partial}{\partial n} \right] \right\};$$

here, $D = 1 + n/r$, r is the radius of curvature of the middle curve of the layer.

Since in our case the radius of curvature of the boundary between the coating layers is much larger than their total thickness, then at the same time, $D \approx 1$ and $\Delta \approx \partial^2/\partial n^2$.

To solve problem (16)–(19), we will use the operator method [147]. Let us enter into Eq. (16):

$$p^2 = \left[\frac{1}{a_2} + \left(\frac{1}{a_3} - \frac{1}{a_2} \right) S_-(n) \right] \frac{\partial}{\partial \tau}$$

Now the equation takes the form

$$\frac{\partial^2 T^*}{\partial n^2} + p^2 T^* = B \delta_-(n), \tag{20}$$

where

$$B = \left(1 - \frac{\lambda_t^{(3)}}{\lambda_t^{(2)}} \right) \frac{\partial T^*}{\partial n} \Big|_{n=0} - \frac{q}{\lambda_t^{(2)}}. \tag{21}$$

The solution of the inhomogeneous Eq. (20) is

$$T^* = D_1 \cos(pn) + D_2 \sin(pn) + \frac{B}{p} \sin(pn) S_-(n). \tag{22}$$

We take the derivative of T^* by n :

$$\frac{\partial T^*}{\partial n} = -pD_1 \sin(pn) + pD_2 \cos(pn) + B \cos(pn) S_-(n) + \frac{B}{p} \sin(pn) \delta_-(n).$$

The last term on the right in the written equation is zero, when $n = 0$, and

$$\frac{\partial T^*}{\partial n} \Big|_{n=0} = pD_2 + B. \tag{23}$$

Substituting (21) into (23), we find $\partial T^*/\partial n|_{n=0}$ and, then, from (21) after transformations, we get

$$B = pD_2 \left(\frac{\lambda_t^{(2)}}{\lambda_t^{(3)}} - 1 \right) - \frac{q}{\lambda_t^{(3)}}. \tag{24}$$

Considering (24), expression (22) takes the following form:

$$\begin{aligned} T^* &= D_1 \cos(pn) + D_2 \sin(pn) + \\ &+ D_2 \left(\frac{\lambda_t^{(2)}}{\lambda_t^{(3)}} - 1 \right) \sin(pn) S_-(n) - \frac{q}{p\lambda_t^{(3)}} \sin(pn) S_-(n). \end{aligned} \tag{25}$$

To find the constants of integration, D_1 and D_2 , we use the first condition (18) and condition (19):

$$\begin{aligned} T^* \Big|_{n=-h_2} &= D_1 \cos(ph_2) - D_2 \sin(ph_2); \\ T^* \Big|_{n=-h_3} &= T_c = D_1 \cos(ph_3) + D_2 \sin(ph_3) + \end{aligned} \tag{26}$$

$$+D_2 \left(\frac{\lambda_t^{(2)}}{\lambda_t^{(3)}} - 1 \right) \sin(ph_3) - \frac{q}{p\lambda_t^{(3)}} \sin(ph_3).$$

After simplifying the system of Eqs. (26), we obtain:

$$T^* \Big|_{n=-h_2} = D_1 \cos(ph_2) - D_2 \sin(ph_2), \tag{27}$$

$$T_c = D_1 \cos(ph_3) + D_2 \frac{\lambda_t^{(2)}}{\lambda_t^{(3)}} \sin(ph_3) - \frac{q}{p\lambda_t^{(3)}} \sin(ph_3).$$

The solution of the system of Eqs. (27) has the form

$$D_1 = \frac{\lambda_t^{(2)} T^* \Big|_{n=-h_2} \sin(ph_3) + \lambda_t^{(3)} T_c \sin(ph_2) + \frac{q}{p} \sin(ph_3) \sin(ph_2)}{\lambda_t^{(2)} \cos(ph_2) \sin(ph_3) + \lambda_t^{(3)} \cos(ph_3) \sin(ph_2)}, \tag{28}$$

$$D_2 = \frac{\lambda_t^{(3)} (T_c \cos(ph_2) - T^* \Big|_{n=-h_2} \cos(ph_3)) + \frac{q}{p} \sin(ph_3) \sin(ph_2)}{\lambda_t^{(2)} \cos(ph_2) \sin(ph_3) + \lambda_t^{(3)} \cos(ph_3) \sin(ph_2)}.$$

We substitute (25) into the second condition (18), take into account (28), as well as the fact that, when $n = -h_2$, $T^* = T$,

$$\begin{aligned} \lambda_t^{(1)} \frac{\partial T}{\partial n} = & \lambda_t^{(2)} p \frac{\left[\lambda_t^{(2)} T \sin(ph_3) + \lambda_t^{(3)} T_c \sin(ph_2) + \frac{q}{p} \sin(ph_3) \sin(ph_2) \right] \sin(ph_2)}{\lambda_t^{(2)} \cos(ph_2) \sin(ph_3) + \lambda_t^{(3)} \cos(ph_3) \sin(ph_2)} + \\ & + \lambda_t^{(2)} p \frac{\left[\lambda_t^{(3)} (T_c \cos(ph_2) - T \cos(ph_3)) + \frac{q}{p} \sin(ph_3) \cos(ph_2) \right] \cos(ph_2)}{\lambda_t^{(2)} \cos(ph_2) \sin(ph_3) + \lambda_t^{(3)} \cos(ph_3) \sin(ph_2)}. \end{aligned} \tag{29}$$

In Eq. (29), T and $\partial T/\partial n$ are taken at $n = -h_2$. We expand the trigonometric functions in Eq. (29) into series and keep, at the same time, only the terms h_2 and h_3 , which also are contained in the first power:

$$\lambda_t^{(1)} \frac{\partial T}{\partial n} = \lambda_t^{(2)} \frac{\lambda_t^{(2)} p^2 h_2 h_3 T}{\lambda_t^{(2)} h_3 + \lambda_t^{(3)} h_2} + \lambda_t^{(2)} \frac{\lambda_t^{(3)} (T_c - T) + q h_3}{\lambda_t^{(2)} h_3 + \lambda_t^{(3)} h_2}. \tag{30}$$

We multiply the left- and right-hand parts of the equation by $\lambda_t^{(2)} h_3 + \lambda_t^{(3)} h_2$ and divide by $\lambda_t^{(2)}$:

$$\frac{\lambda_t^{(1)}}{\lambda_t^{(2)}} (\lambda_t^{(2)} h_3 + \lambda_t^{(3)} h_2) \frac{\partial T}{\partial n} = \lambda_t^{(2)} h_2 h_3 p^2 T + \lambda_t^{(3)} (T_c - T) + q h_3. \tag{31}$$

In Eq. (31), we substitute p^2 :

$$p^2 = -\frac{1}{a_2} \frac{\partial}{\partial \tau};$$

then, we get

$$\frac{\lambda_t^{(1)}}{\lambda_t^{(2)}} (\lambda_t^{(2)} h_3 + \lambda_t^{(3)} h_2) \frac{\partial T}{\partial n} + \frac{\lambda_t^{(2)}}{a_2} h_2 h_3 \frac{\partial T}{\partial \tau} + \lambda_t^{(3)} T = \lambda_t^{(3)} T_c + q h_3. \quad (32)$$

We divide the left- and right-hand parts of Eq. (32) by h_3 and obtain the heat-exchange condition at the boundary between the steel cylinder and the unoxidized layer of aluminium ($n = -h_2$):

$$\lambda_t^{(1)} \left(1 + \frac{R_2}{R_3} \right) \frac{\partial T}{\partial n} + C_2 \frac{\partial T}{\partial \tau} + \frac{1}{R_3} T = \frac{1}{R_3} T_c + q, \quad (33)$$

where $R_i = h_i/\lambda_t^{(i)}$ is the thermal resistance of the i -th layer ($i = 2, 3$); $C_2 = c_v^{(2)} h_2$, $c_v^{(2)}$ is volumetric heat capacity of the 2nd layer [J/(m³·deg)] (C_2 is heat capacity of 1 m² of the 2nd layer [J/(m²·deg)]). The thermal resistance of the i -th layer is the temperature difference that occurs when a unit heat flow (1 W/m²) passes through it.

We make sure that the boundary condition (32) is correct. It is obvious that the power of the cylindrical heat source q , which is located at the border of the 2nd and 3rd layers of the coating, causes the heating of these layers and, in addition, the heating of the steel cylinder itself, the radius of which is r_1 .

Let us solve equation (33) with respect to q :

$$q = \lambda_t^{(1)} \left(1 + \frac{R_2}{R_3} \right) \frac{\partial T}{\partial n} + C_2 \frac{\partial T}{\partial \tau} - \frac{1}{R_3} (T_b - T) + \frac{1}{R_3} (T_b - T_c). \quad (34)$$

In Eq. (34), $\lambda_t^{(1)} \partial T / \partial n$ is the value of the heat flow that goes to heat the steel cylinder; $C_2 \partial T / \partial \tau$ is the amount of heat that remains in 1 m² of the 2nd layer per unit of time and causes its temperature to rise; T_b is temperature of the boundary between the 2nd and 3rd layers; $(T_b - T_c) / R_3$ is the amount of heat entering 1 m² of the 3rd layer per unit of time [W/m²].

The sum of the terms remaining on the right in Eq. (34) must be zero, if the heat exchange condition (33) is valid, namely,

$$\lambda_t^{(1)} \frac{R_2}{R_3} \frac{\partial T}{\partial n} - \frac{1}{R_3} (T_b - T) = \frac{R_2}{R_3} \left(\lambda_t^{(1)} \frac{\partial T}{\partial n} - \lambda_t^{(2)} \frac{T_b - T_c}{h_2} \right).$$

With a thin layer 2, the law of temperature change in it is almost linear; therefore,

$$\lambda_t^{(2)} \frac{T_b - T}{h_2} \approx \lambda_t^{(2)} \frac{\partial T^*}{\partial n};$$

this means, because of the second condition of ideal thermal contact (18), that the expression in round brackets is equal to zero. That is, the heat exchange condition (33) fully coincides with the physical picture of

heat distribution, which is generated by a cylindrical heat source located at the boundary between the second and third layers.

3. Results and Discussion

3.1. Determination of the Temperature in a Steel Cylinder

Using the obtained heat transfer condition (33), it is now possible to formulate the problem of temperature field distribution for a steel cylinder:

$$\frac{\partial T}{\partial \tau} = a \left(\frac{\partial^2 T}{\partial r^2} + \frac{1}{r} \frac{\partial T}{\partial r} \right), \quad 0 \leq r \leq r_1; \quad (35)$$

$$T|_{\tau=0} = T_0; \quad (36)$$

$$\lambda_t \left(1 + \frac{R_2}{R_3} \right) \frac{\partial T}{\partial r} \Big|_{r=r_1} + C_2 \frac{\partial T}{\partial r} \Big|_{r=r_1} + \frac{1}{R_3} \frac{\partial T}{\partial r} \Big|_{r=r_1} = \frac{T_c}{R_3} + q; \quad (37)$$

$$T|_{r=0} \neq \infty; \quad (38)$$

here, a is coefficient of temperature conductivity of the cylinder [m^2/s]; λ_t is thermal conductivity coefficient of the cylinder ($\lambda_t = \lambda_t^{(1)}$).

To solve the problem (35)–(38), we used the integral Laplace transform [145]. One of the most powerful generalizations of this transformation is the Laplace–Stieltjes integral [154, 155]. We apply this transformation to Eqs. (35)–(38):

$$s\bar{T} - T_0 = a \left(\frac{d^2 \bar{T}}{dr^2} + \frac{1}{r} \frac{d\bar{T}}{dr} \right), \quad (39)$$

$$\lambda_t \left(1 + \frac{R_2}{R_3} \right) \frac{\partial \bar{T}}{\partial r} \Big|_{r=r_1} + C_2 (s\bar{T}|_{r=r_1} - T_0) + \frac{1}{R_3} \bar{T} \Big|_{r=r_1} = \frac{T_c}{sR_3} + \frac{q}{s}, \quad (40)$$

$$\bar{T} \Big|_{r=0} \neq \infty, \quad (41)$$

where s is parameter of Laplace transform.

The solution of Eq. (39) has the following form [145]:

$$\bar{T} - \frac{T_0}{s} = A_1 I_0 \left(\sqrt{\frac{s}{a}} r \right) + A_2 K_0 \left(\sqrt{\frac{s}{a}} r \right), \quad (42)$$

where $I_0(x)$, $K_0(x)$ are modified zero-order Bessel functions.

To find the integration constants A_1 and A_2 , we use the boundary conditions (37) and (38):

$$\lambda_t \left(1 + \frac{R_2}{R_3} \right) A_1 I_1 \left(\sqrt{\frac{s}{a}} r_1 \right) \sqrt{\frac{s}{a}} - \lambda_t \left(1 + \frac{R_2}{R_3} \right) A_2 \sqrt{\frac{s}{a}} K_1 \left(\sqrt{\frac{s}{a}} r_1 \right) +$$

$$\begin{aligned}
 &+ C_2 S \left[A_1 I_0 \left(\sqrt{\frac{s}{a}} r_1 \right) + A_2 K_0 \left(\sqrt{\frac{s}{a}} r_1 \right) \right] + \tag{43} \\
 &+ \frac{1}{R_3} \left[A_1 I_0 \left(\sqrt{\frac{s}{a}} r_1 \right) + A_2 K_0 \left(\sqrt{\frac{s}{a}} r_1 \right) + \frac{T_0}{s} \right] = \frac{T_c}{s R_3} + \frac{q}{s}.
 \end{aligned}$$

It follows from the boundary condition (41) that, since $A_2 = 0$, at $r \rightarrow 0$, $K_0 \left(\frac{s}{a} r \right) \rightarrow -\infty$. So,

$$\bar{T} = A_1 I_0 \left(\sqrt{\frac{s}{a}} r \right) + \frac{T_0}{s}, \tag{44}$$

and therefore, condition (42) is

$$A_1 \left[\lambda_t \left(1 + \frac{R_2}{R_3} \right) \sqrt{\frac{s}{a}} I_1 \left(\sqrt{\frac{s}{a}} r_1 \right) + \left(C_2 s + \frac{1}{R_3} \right) I_0 \left(\sqrt{\frac{s}{a}} r_1 \right) \right] = \frac{T_c - T_0}{s R_3} + \frac{q}{s}. \tag{45}$$

Hence,

$$A_1 = \frac{(T_c - T_0) / R_3 + q}{s \left[\lambda_t \left(1 + \frac{R_2}{R_3} \right) \sqrt{\frac{s}{a}} I_1 \left(\sqrt{\frac{s}{a}} r_1 \right) + \left(C_2 s + \frac{1}{R_3} \right) I_0 \left(\sqrt{\frac{s}{a}} r_1 \right) \right]}. \tag{46}$$

Now the Laplace transform of the temperature function in the cylinder is written as

$$\bar{T} = \frac{\left(\frac{T_c - T_0}{R_3} + q \right) I_0 \left(\sqrt{\frac{s}{a}} r \right)}{s \left[\lambda_t \left(1 + \frac{R_2}{R_3} \right) \sqrt{\frac{s}{a}} I_1 \left(\sqrt{\frac{s}{a}} r_1 \right) + \left(C_2 s + \frac{1}{R_3} \right) I_0 \left(\sqrt{\frac{s}{a}} r_1 \right) \right]} + \frac{T_0}{s}. \tag{47}$$

Expression (47) satisfies both differential Eq. (39) and boundary conditions (40) and (41). To obtain the original of the function (47), it is necessary to perform the inverse transformation over the function \bar{T} . Expression (47) is the ratio of two generalized polynomials with respect to s , while the denominator power is greater than that of the numerator and does not contain a constant. In addition, this means that the decomposition theorem may be used to find the inverse transformation of the function (47).

To apply the decomposition theorem, the roots of the denominator in (47) are found:

$$\beta_{(s)} = s \left[\lambda_t \left(1 + \frac{R_2}{R_3} \right) \sqrt{\frac{s}{a}} I_1 \left(\sqrt{\frac{s}{a}} r_1 \right) + \left(C_2 s + \frac{1}{R_3} \right) I_0 \left(\sqrt{\frac{s}{a}} r_1 \right) \right] = s \varphi_{(s)} = 0. \tag{48}$$

From Eq. (48), the roots are: (1) $s_0 = 0$; (2) $\varphi_s = 0$. Herefrom, $s_n = -\frac{a\mu_n^2}{r_1^2}$, $\mu_n = i\sqrt{\frac{s}{a_1}} r_1$ ($n = 1, 2, 3, \dots$).

The transition to ordinary Bessel functions is carried out as follows:

$$I_1(z) = i^{-1}J_1(iz), I_0(z) = J_0(iz),$$

where i is an imaginary unit, that is, $i^2 = -1$.

From the last equation after transformations, we get:

$$\lambda_t \left(1 + \frac{R_2}{R_3} \right) J_1(\mu) + \left(C_2 \frac{a\mu}{r_1} - \frac{r_1}{R_3\mu} \right) J_0(\mu) = 0. \quad (49)$$

Equation (49) has many roots μ_n ($n = 1, 2, 3, \dots$) that means that there will be many roots for S_n .

The inverse Laplace transform of function (47), using the decomposition theorem [145, 156], will be:

$$T = T_0 + \frac{\psi(0)}{\varphi(0)} + \sum_{n=1}^{\infty} \frac{\psi(s_n)}{s_n \varphi'(s_n)} e^{s_n \tau}, \quad (50)$$

where

$$\psi(s) = ((T_c - T_0) / R_3 + q) I_0 \left(\sqrt{\frac{s}{a}} r \right),$$

$$\varphi(s) = \lambda_t \left(1 + \frac{R_2}{R_3} \right) \sqrt{\frac{s}{a}} I_1 \left(\sqrt{\frac{s}{a}} r_1 \right) + \left(C_2 s + \frac{1}{R_3} \right) I_0 \left(\sqrt{\frac{s}{a}} r_1 \right).$$

Here,

$$\psi(0) = \frac{T_c - T_0}{R_3} + q, \quad \varphi(0) = \frac{1}{R_3},$$

$$\begin{aligned} \varphi'(s) = \lambda_t \left(1 + \frac{R_2}{R_3} \right) & \left[\frac{1}{2\sqrt{sa}} I_1 \left(\sqrt{\frac{s}{a}} r_1 \right) + \sqrt{\frac{s}{a}} \frac{r_1}{2\sqrt{sa}} \frac{1}{2} \left(I_0 \left(\sqrt{\frac{s}{a}} r_1 \right) + I_2 \left(\sqrt{\frac{s}{a}} r_1 \right) \right) \right] + \\ & + C_2 I_0 \left(\sqrt{\frac{s}{a}} r_1 \right) + \left(C_2 s + \frac{1}{R_3} \right) \frac{r_1}{2\sqrt{sa}} I_1 \left(\sqrt{\frac{s}{a}} r_1 \right). \end{aligned}$$

After transformations, the last expression is

$$\varphi'(s) = \left[\lambda_t \left(1 + \frac{R_2}{R_3} \right) \frac{r_1}{2a} + C_2 \right] I_0 \left(\sqrt{\frac{S}{a}} r_1 \right) + \frac{(C_2 S + 1 / R_3) r_1}{2\sqrt{Sa}} I_1 \left(\sqrt{\frac{S}{a}} r_1 \right). \quad (51)$$

As a result of the transformations, formula (50) is

$$T = T_c + qR_3 + \sum_{n=1}^{\infty} \frac{((T_c - T_0) / R_3 + q)I_0(i\mu_n r / r_1)e^{-\frac{a\mu_n^2}{r_1^2}\tau}}{\left[\lambda_t \left(1 + \frac{R_2}{R_3} \right) \frac{r_1}{2a} + C_2 \right] I_0(i\mu_n) + \frac{\left(-C_2 \frac{a\mu_n^2}{r_1^2} + 1 / R_3 \right) r_1}{2ia\mu_n / r_1} I_1(i\mu_n) \right]} \quad (52)$$

After transformations of the last expression, we get:

$$T = T_c + qR_3 - 2(T_c - T_0 + qR_3) \frac{r_1^2}{a} \times \sum_{n=1}^{\infty} \frac{J_0\left(\frac{\mu_n r}{r_1}\right) e^{-\frac{a\mu_n^2}{r_1^2}\tau}}{\mu_n^2 \left\{ \left[\lambda_t (R_2 + R_3) \frac{r_1}{a} + 2C_2 R_3 \right] J_0(\mu_n) + \left(\frac{r_1^2}{a\mu_n} - C_2 R_3 \right) J_1(\mu_n) \right\}} \quad (53)$$

Here, $J_0(\mu_n r / r_1)$, $J_1(\mu_n)$ are Bessel functions of zero and first order. Considering that Bessel functions have a bounded index, a series of function (51) with coefficients of a bounded index in the theory of functions was first studied by Lepson [157] (see also Ref. [158]).

Let us make sure that the expression (53) is indeed a solution of the boundary value problem (35)–(38). Firstly check, whether (53) satisfies the differential Eq. (35):

$$\frac{\partial T}{\partial r} = 2(T_c - T_0 + qR_3) \frac{r_1^2}{a} \sum_{n=1}^{\infty} \frac{\mu_n J_1\left(\frac{\mu_n r}{r_1}\right) e^{-\frac{a\mu_n^2}{r_1^2}\tau}}{f(\mu_n)}, \quad (54)$$

where

$$f(\mu_n) = \mu_n^2 \left\{ \left[\lambda_t (R_2 + R_3) \frac{r_1}{a} + 2C_2 R_3 \right] J_0(\mu_n) + \left(\frac{r_1^2}{a\mu_n} - C_2 R_3 \mu_n \right) J_1(\mu_n) \right\},$$

$$\frac{\partial^2 T}{\partial r^2} = 2(T_c - T_0 + qR_3) \frac{r_1^2}{a} \sum_{n=1}^{\infty} \frac{\frac{\mu_n^2}{r_1^2} \left[J_0\left(\mu_n \frac{r}{r_1}\right) - \frac{r_1}{\mu_n r} J_1\left(\mu_n \frac{r}{r_1}\right) \right]}{f(\mu_n)} e^{-\frac{a\mu_n^2}{r_1^2}\tau}, \quad (55)$$

$$\frac{\partial T}{\partial \tau} = 2(T_c - T_0 + qR_3) \frac{r_1^2}{a} \sum_{n=1}^{\infty} \frac{J_0\left(\mu_n \frac{r}{r_1}\right) a\mu_n^2 e^{-\frac{a\mu_n^2}{r_1^2}\tau}}{f(\mu_n)}. \quad (56)$$

Let us substitute (54) and (55) into the right side of Eq. (35):

$$a \left(\frac{\partial^2 T}{\partial r^2} + \frac{1}{r} \frac{\partial T}{\partial r} \right) =$$

$$\begin{aligned}
 &= 2(T_c - T_0 + qR_3)r_1^2 \sum_{n=1}^{\infty} \frac{\frac{\mu_n^2}{r_1^2} \left[J_0\left(\mu_n \frac{r}{r_1}\right) - \frac{r_1}{\mu_n r} J_1\left(\frac{\mu_n r}{r_1}\right) \right]}{f(\mu_n)} e^{-\frac{a\mu_n^2}{r_1^2}\tau} + \quad (57) \\
 &+ 2(T_c - T_0 + qR_3)r_1^2 \sum_{n=1}^{\infty} \frac{\frac{\mu_n}{r_1} J_1\left(\mu_n \frac{r}{r_1}\right) e^{-\frac{a\mu_n^2}{r_1^2}\tau}}{f(\mu_n)} = \\
 &= 2(T_c - T_0 + qR_3)r_1^2 \sum_{n=1}^{\infty} \frac{J_0\left(\frac{\mu_n r}{r_1}\right) \frac{\mu_n^2}{r_1^2} e^{-\frac{a\mu_n^2}{r_1^2}\tau}}{f(\mu_n)}.
 \end{aligned}$$

The result in Eq. (57) is equal to (56) that means that (53) satisfies the differential Eq. (35).

It is analytically difficult to verify the validity of the initial condition (36). This condition will be verified numerically later.

Let us consider the boundary condition (37):

$$\begin{aligned}
 \left. \frac{\partial T}{\partial r} \right|_{r=r_1} &= 2(T_c - T_0 + qR_3) \frac{r_1^2}{a} \sum_{n=1}^{\infty} \frac{\frac{\mu_n}{r_1} J_1(\mu_n) e^{-\frac{a\mu_n^2}{r_1^2}\tau}}{f(\mu_n)}; \\
 \left. \frac{\partial T}{\partial \tau} \right|_{r=r_1} &= 2(T_c - T_0 + qR_3)r_1^2 \sum_{n=1}^{\infty} \frac{J_0(\mu_n) \frac{\mu_n^2}{r_1^2} e^{-\frac{a\mu_n^2}{r_1^2}\tau}}{f(\mu_n)}; \\
 T|_{r=r_1} &= T_c + qR_3 - 2(T_c - T_0 + qR_3) \frac{r_1^2}{a} \sum_{n=1}^{\infty} \frac{J_0(\mu_n) e^{-\frac{a\mu_n^2}{r_1^2}\tau}}{f(\mu_n)}.
 \end{aligned}$$

Substituting the obtained values $\partial T/\partial r|_{r=r_1}$, $\partial T/\partial \tau|_{r=r_1}$, $T|_{r=r_1}$, into the boundary condition (37), we have:

$$\begin{aligned}
 &2(T_c - T_0 + qR_3) \frac{r_1^2}{a} \sum_{n=1}^{\infty} \frac{\lambda_t \left(1 + \frac{R_2}{R_3}\right) \frac{r_n}{r_1} J_1(\mu_n) e^{-\frac{a\mu_n^2}{r_1^2}\tau}}{f(\mu_n)} + \\
 &+ 2(T_c - T_0 + qR_3) r_1^2 \sum_{n=1}^{\infty} \frac{C_2 J_0(\mu_n) \frac{r_n^2}{r_1^2} e^{-\frac{a\mu_n^2}{r_1^2}\tau}}{f(\mu_n)} +
 \end{aligned}$$

$$\begin{aligned}
 & + \frac{T_c + qR_3}{R_3} - 2(T_c - T_0 + qR_3) \frac{r_1^2}{a} \sum_{n=1}^{\infty} \frac{R_3}{R_3} \frac{J_0(\mu_n) e^{-\frac{a\mu_n^2 \tau}{r_1^2}}}{f(\mu_n)} = \\
 & = \frac{T_c}{R_3} + q + 2(T_c - T_0 + qR_3) \frac{r_1^2}{a} \times \\
 & \times \sum_{n=1}^{\infty} \frac{\mu_n \left[\lambda_t \left(1 + \frac{R_2}{R_3} \right) J_1(\mu_n) + \left(C_2 \frac{a\mu_n}{r_1} - \frac{r_1}{R_3\mu_n} \right) J_0(\mu_n) \right] e^{-\frac{a\mu_n^2 \tau}{r_1^2}}}{f(\mu_n)}.
 \end{aligned}$$

The expression in square brackets under the sum sign is equal to zero, since $\{\mu_n\}$ are the roots of Eq. (49), i.e.,

$$\lambda_t \left(1 + \frac{R_2}{R_3} \right) \frac{\partial T}{\partial r} \Big|_{r=r_1} + C_2 \frac{\partial T}{\partial \tau} \Big|_{r=r_1} + \frac{1}{R_3} T \Big|_{r=r_1} = \frac{T_c}{R_3} + q.$$

This means that Eq. (53) satisfies the boundary condition (37).

Condition (38) is also satisfied by expression (53), because the numerator in Eq. (53) rapidly approaches zero as μ_n increases.

To perform calculations of the temperature field in the cylinder according to the formula (53) and to check, if the analytical expression (53) really satisfies the initial condition (36), the following initial data were taken:

(1) thermal conductivity coefficient of steel grade 45

$$\lambda = 38 \text{ W}/(\text{m} \cdot \text{deg}) \text{ [159]};$$

(2) volumetric heat capacity of aluminium

$$C_v^2 = c^{(2)}\rho^{(2)} = 896.4 \cdot 2680 = 2402352 \text{ J}/(\text{m}^3 \cdot \text{deg}),$$

where c_2 is specific heat capacity of aluminium (896.4 W/(m³·deg)), $\rho^{(2)}$ is density of aluminium (2680 kg/m³ [159]);

(3) average aluminium layer thickness formed during PEO

$$h_2 = 0.318 \cdot 10^{-3} \text{ m};$$

(4) heat capacity of 1 m² of the second layer (aluminium)

$$C_2 = C_v^{(2)} \cdot h_2 = 2402352 \cdot 0.318 \cdot 10^{-3} = 763.948 \text{ J}/(\text{m}^2 \cdot \text{deg});$$

(5) temperature resistance of the second layer (aluminium)

$$R_2 = \frac{h_2}{\lambda_t^{(2)}}, \lambda_t^{(2)} = 209 \text{ W}/(\text{m} \cdot \text{deg}) \text{ [159]},$$

$$R_2 = \frac{0.318 \cdot 10^{-3}}{209} = 1.521531 \cdot 10^{-6} \text{ (m}^2 \cdot \text{deg)}/\text{W};$$

(6) coefficient of temperature conductivity of steel grade 45

$$a = 27 \cdot 10^{-3} = \text{m}^2/\text{h} = 7.5 \cdot 10^{-6} \text{ m}^2/\text{s};$$

(7) temperature resistance of the third layer (aluminium oxide)

$$R_3 = \frac{h_3}{\lambda_t^{(3)}} = \frac{0.282 \cdot 10^{-3}}{21.2829} = 1.325007 \cdot 10^{-5} \text{ (m}^2 \cdot \text{deg)/W,}$$

where h_3 is the average thickness of the aluminium-oxide (Al₂O₃) layer formed during PEO ($h_3 = 0.282 \cdot 10^{-3}$ m), $\lambda_t^{(3)}$ is coefficient of thermal conductivity of aluminium oxide ($\lambda_t^{(3)} = 21.2829$ W/(m·deg) [160]);

(8) power of the PEO process

$$P = \frac{kiU}{\sqrt{2}} \text{ [W/dm}^2\text{]},$$

where i is current density during PEO ($i = 5$ A/dm²), U is voltage during PEO ($U = 760$ V), k is coefficient taking into account the part of the power that goes to heating the three-layer cylinder; so,

$$P = \frac{0.7 \cdot 5 \cdot 760}{\sqrt{2}} = 1800.9 \text{ W/dm}^2 = 188090 \text{ W/m}^2;$$

(9) temperature of the electrolyte is assumed constant and is equal to $T_c = 70$ °C.

Taking into account the accepted initial data, during the numerical verification of the initial condition (36), it was established that at the initial moment of time the temperature at all points of the cylinder is equal to 20 °C.

When calculating the temperature distribution in the cylinder depending on the radius of the cylinder points and the time from the beginning of the PEO process (heating), results were obtained, which show that, after a relatively short period of time ($\tau = 180$ s) from the beginning of the PEO, the temperature at all points of the cylinder becomes the same, *i.e.*, a steady state occurs in the cylinder. The obtained temperature ($T = 72.49$ °C) is a stationary temperature arising from the action of the surface cylindrical heat source, which is located at the boundary of the aluminium-oxide and aluminium layers (Fig. 4). In reality, during PEO, we do not have a cylindrical heat source, but practically instantaneous point sources of heat of extremely low thermal energy $Q = 0.002$ J, which act at different points of the cylindrical surface at the boundary of the aluminium-oxide layer and the aluminium layer (the position of these points, obviously, continuously changes) so densely and with very small time intervals between successive flashes of discharges so that the temperature on each cylindrical surface remote from the heat sources in the middle of the steel cylinder is constant. After a short period, the temperatures on all these cylindrical surfaces equalize and become equal to 72.49 °C. Only in a small layer of aluminium directly adjacent to the edge cylindrical surface of the steel cylinder radius r_1 , we will have a non-stationary temperature, since this layer is in close proximity to the action of instantaneous point heat

sources during PEO (they are separated by a thin unoxidized layer of aluminium).

It is of great interest to find out what temperatures are possible on the outer surface of a steel cylinder? As known from the PEO technological process, in the final stage of it, the thickness of the aluminium layer applied to the steel cylinder decreases to the size of the unoxidized layer (of 35–65 μm). This interest is explained by the fact that, at a temperature T equal to $0.4T_m$ of the metal (T_m is a melting T), diffusion processes occur from steel to aluminium and vice versa. It is necessary to theoretically confirm or deny the phenomenon of diffusion at the boundary between an unoxidized layer of aluminium and a steel cylinder. It is not possible to establish the real temperature field in the cylinder caused by instantaneous point sources, since there is no reliable data in the literature about the frequency of their occurrence and their distribution over the entire surface of the aluminium layer during PEO.

The calculated temperature field in the cylinder coincides with its real temperature field during the PEO process with the exception of a small layer adjacent to the edge surface of the cylinder radius (Fig. 4). If the PEO process is stopped, then, after an extremely short period of time (hundredths of a second), the temperature in this layer will also be equal to 72.49 $^{\circ}\text{C}$.

The results of measuring the temperature distribution of the electrolyte during PEO of aluminium alloy by a thermal imaging camera [161] show that the minimum temperature near the stainless steel electrode is of 46.6 $^{\circ}\text{C}$, and the maximum temperature is of 92.7 $^{\circ}\text{C}$ in the area, where the rectangular aluminium part is located.

3.2. Determination of the Temperature for the Half-Space

To obtain a good approximation of the real temperature field in an unoxidized aluminium thin layer of a cylinder experiencing heating by instantaneous point heat sources during PEO, let us consider the following temperature problem for a half-space. At the initial moment of time, the temperature at all points of the half-space is the same and is equal to T_0 . The temperature at the edge of the half-space ($z = 0$) is constant and equal to T_0 . An instantaneous point source of heat acts at the point with coordinates $x = y = 0$ and $z = z_1$. However, this source of heat does not work continuously, but only at moments of time $\tau = \tau_1, \tau_2, \tau_3$ and τ_4 . It is necessary to establish the temperature field distribution in the half-space.

Why is a point heat source considered in a half-space and not in a cylinder? The following explanation may be given here. The energy of an instantaneous point source during a discharge is extremely small and it causes a temperature change in a very small volume, which means

that the geometry of the body will not affect the temperature in that volume. It follows that there is no need to consider the temperature problem for a cylinder with point sources, since its solution is significantly more complicated than for a half-space, and the result will be practically the same.

The temperature T_0 can be taken as the stationary temperature in the cylinder ($T = 72.49$ °C) and the co-ordinate z can be taken equal to the distance of the cylindrical source to the outer surface of the aluminium-oxide layer, *i.e.*, $z_1 = h_3$. Under this condition, the temperature occurring at distances of 35–65 μm from the instantaneous point source deep into the half-space is approximately that occurring on the surface of a steel cylinder at the final stage of the PEO process.

The formulated problem may be mathematically written as follows:

$$\frac{\partial T}{\partial \tau} = 2(T_c - T_0 + qR_3) \frac{r_1^2}{a} \sum_{n=1}^{\infty} \frac{J_0\left(\mu_n \frac{r}{r_1}\right) \frac{a\mu_n^2}{r_1^2} e^{-\frac{a\mu_n^2}{r_1^2}\tau}}{f(\mu_n)},$$

$$\frac{\partial^2 T}{\partial x^2} + \frac{\partial^2 T}{\partial y^2} + \frac{\partial^2 T}{\partial z^2} = \frac{1}{a} \frac{\partial T}{\partial \tau} - \frac{Q}{\lambda_t} \delta(x) \delta(y) \delta(z - z_1) \sum_{i=1}^4 \delta(\tau - \tau_i) \quad (58)$$

under initial conditions:

$$T|_{\tau=0} = T_0, T|_{z=0} = T_0, T|_{z \rightarrow \infty} \rightarrow T_0; \quad (59)$$

here, T is temperature field in half-space; x, y, z are co-ordinates of half-space points; τ is time; λ_t, a are the coefficients of material thermal conductivity and temperature conductivity of the half-space, respectively (we take aluminium as the material of the half-space); Q is energy of an instantaneous point source [J]; Dirac delta functions [144] are: $\delta(x), \delta(y), \delta(z - z_1), \delta(\tau - \tau_i)$.

To ensure the possibility of applying Fourier integral transforms, a new function of T_1 is added to consideration:

$$T_1 = T - T_0. \quad (60)$$

Let us express T through T_1 and substitute into Eqs. (58) and (59). Therefore, the result is

$$\frac{\partial^2 T_1}{\partial x^2} + \frac{\partial^2 T_1}{\partial y^2} + \frac{\partial^2 T_1}{\partial z^2} = \frac{1}{a} \frac{\partial T_1}{\partial \tau} - \frac{Q}{\lambda_t} \delta(x) \delta(y) \delta(z - z_1) \sum_{i=1}^4 \delta(\tau - \tau_i) \quad (61)$$

for such conditions:

$$T_1|_{\tau=0} = 0, T_1|_{z=0} = 0, T_1|_{z \rightarrow \infty} \rightarrow 0. \quad (62)$$

We solve problem (61), (62), using the Fourier exponential transform [145, 146]

$$\bar{f}(\xi) = \frac{1}{\sqrt{2\pi}} \int_{-\infty}^{\infty} f(x) e^{i\xi x} dx \quad (63)$$

by the variables x and y , as well as the sine Fourier transform [145, 146]

$$\overline{F}(p) = \sqrt{\frac{2}{\pi}} \int_0^\infty F(z) \sin(pz) dz \tag{64}$$

by variable z .

As a result of applying transformation (63) to Eqs. (61), (62) by variables x and y , we obtain

$$-(\xi^2 + \zeta^2) \overline{\overline{T_1}} + \frac{\partial^2 \overline{\overline{T_1}}}{\partial z^2} = \frac{1}{a} \frac{\partial \overline{\overline{T_1}}}{\partial \tau} - \frac{Q}{2\pi\lambda_t} \delta(z - z_1) \sum_{i=1}^4 \delta(\tau - \tau_i), \tag{65}$$

$$T_{1/\tau=0} = 0, T_{1/z=0} = 0, T_{1/z \rightarrow \infty} \rightarrow 0, \tag{66}$$

where $\overline{\overline{T_1}}$ is double integral Fourier transform of a function T_1 ; ξ, ζ are parameters of integral transformations, respectively.

Next, we use the integral transformation (64) to Eqs. (65), (66) by variable z and obtain:

$$\frac{d \overline{\overline{T_1}}}{d\tau} + a(\xi^2 + \zeta^2 + p^2) \overline{\overline{T_1}} = \frac{Qa}{\sqrt{2\pi^3\lambda_t}} \sin(pz_1) \sum_{i=1}^4 \delta(\tau - \tau_i), \tag{67}$$

$$\overline{\overline{T_1}}_{\tau=0} = 0. \tag{68}$$

The solution of Eq. (67) under condition (68) has the following form:

$$\overline{\overline{T_1}} = \frac{Qa}{\sqrt{2\pi^3\lambda_t}} \sin(pz_1) \sum_{i=1}^4 e^{-(\xi^2 + \zeta^2 + p^2)(\tau - \tau_i)} U(\tau - \tau_i), \tag{69}$$

where $U(\tau - \tau_i)$ is the Heaviside function [144].

We use inverse integral transformations. So, inverse sine Fourier transform

$$\begin{aligned} \overline{\overline{T_1}} &= \sqrt{\frac{2}{\pi}} \int_0^\infty \overline{\overline{T_1}} \sin(pz) dp = \\ &= \frac{Qa}{\pi^2\lambda_t} \sum_{i=1}^4 e^{-a(\xi^2 + \zeta^2)(\tau - \tau_i)} U(\tau - \tau_i) \int_0^\infty e^{-ap^2(\tau - \tau_i)} \sin(pz_1) \sin(pz) dp. \end{aligned}$$

After taking the last integral, we get [162]

$$\overline{\overline{T_1}} = \frac{Qa}{4\lambda_t} \sum_{i=1}^4 \sqrt{\frac{1}{\pi^3 a(\tau - \tau_i)}} e^{-a(\xi^2 + \zeta^2)(\tau - \tau_i)} U(\tau - \tau_i) \left[e^{-\frac{(z-z_1)^2}{4a(\tau - \tau_i)}} - e^{-\frac{(z+z_1)^2}{4a(\tau - \tau_i)}} \right]. \tag{70}$$

Next, we perform inverse exponential Fourier transformations:

$$\overline{\overline{T_1}} = \frac{1}{\sqrt{2\pi}} \int_{-\infty}^\infty \overline{\overline{T_1}} e^{-i\zeta y} d\zeta, T_1 = \frac{1}{\sqrt{2\pi}} \int_{-\infty}^\infty \overline{\overline{T_1}} e^{-i\xi x} d\xi.$$

As a result, the solution of problem (61), (62) takes the form

$$T_1 = \frac{Q a}{\lambda_t} \sum_{i=1}^4 \frac{U(\tau - \tau_i)}{(2\sqrt{\pi a(\tau - \tau_i)})^3} e^{-\frac{x^2+y^2}{4a(\tau-\tau_i)}} \left[e^{-\frac{(z-z_1)^2}{4a(\tau-\tau_i)}} - e^{-\frac{(z+z_1)^2}{4a(\tau-\tau_i)}} \right]. \quad (71)$$

To calculate the temperature T ($T = T_1 + T_0$) in the half-space, formula (71) and the initial temperature T_0 were used. Calculations were performed for different moments of time τ and different values of coordinates z and x close to the point of flash of an instantaneous point source of heat (single discharge during PEO). The specified point source flashes at a point in the half-space with coordinates $x = y = 0$ and $z = z_1$ at the time instant: $\tau_1, \tau_2, \tau_3, \tau_4$.

During the calculations, the following input data were taken: the material of the half-space is aluminium; energy of an instantaneous point heat source $Q = 0.002$ J; coefficients of thermal conductivity and temperature conductivity of aluminium, respectively, $\lambda_t = 255/(m \cdot \text{deg})$, $a = 9.2592592 \cdot 10^{-5}$ m²/s; moments of flash of an instantaneous point source of heat (spark discharge): $\tau_1 = 0$ s, $\tau_2 = 0.01$ s, $\tau_3 = 0.02$ s, $\tau_4 = 0.03$ s; co-ordinates of the instantaneous point source of heat: $x = y = 0$, $z = z_1 = 0.282 \cdot 10^{-3}$ m; the initial temperature in the half-space $T_0 = 72.49$ °C.

The obtained calculation results indicate that, with a thickness of the unoxidized aluminium layer from 0.035 to 0.040 mm, the temperature on the steel cylinder surface after flashes of instantaneous new point heat sources during PEO exceeds 1000 °C. This means that the

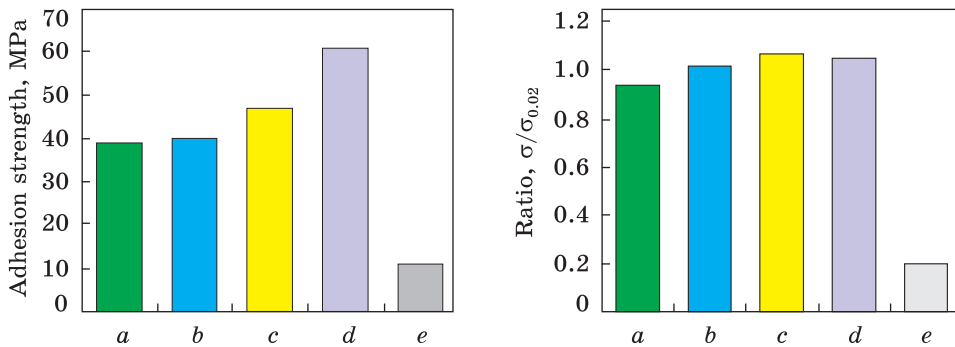


Fig. 5. The adhesion strength with the steel substrate of the one-layer Al coating with a thickness of 250 μm (a) and the two-layer Al–Al₂O₃ coating with a thickness of 250 μm with different thickness of the unoxidized Al layer: 125 μm (b); 65 μm (c); 35 μm (d); 0 μm (e)

Fig. 6. The static resistance to sulphide stress cracking of carbon steel 45 with one-layer Al coating with a thickness of 250 μm (a) and two-layer Al–Al₂O₃ coating with a thickness of 250 μm with different thickness of the unoxidized Al layer: 125 μm (b); 65 μm (c); 35 μm (d); 0 μm (e)

mutual diffusion of iron from steel to aluminium and vice versa will take place in the layers of these composition materials adjacent to their contact surface, which will ensure the emergence of a diffuse connection (welding) of the applied layer of aluminium to the steel base in a two-layer coating: lower — unoxidized layer of aluminium, outer — aluminium oxide layer formed in the PEO process.

The results of studies [163, 164] show that diffusion processes, especially grain boundary diffusion, begin to occur in aluminium alloys at elevated temperatures ($T > 0.4T_m$, where T_m is the melting temperature of the alloy). Such diffusion phenomena will contribute to the possibility of forming a metallurgical bond between the aluminium layer and the steel, which ensures a significant increase in the adhesion strength of the two-layer Al–Al₂O₃ coating to the steel substrate. In particular, the work [165] is devoted to the study of the processes of the diffusion connection of an aluminium alloy with steel. The results indicate that metallurgical bonding can be observed between the coatings and the steel substrate.

3.3. Results of the Mechanical, Tribological and Stress Corrosion Cracking Testing

The results of testing samples for the adhesion strength of coatings to a steel base are presented in Fig. 5. With a thickness of the unoxidized Al layer of 125 μm (Fig. 5, *b*), the adhesion strength of the coating to the base is of 40 MPa and is practically the same as for a single-layer Al coating with a thickness of 250 μm without PEO, namely, of 39 MPa (Fig. 5, *a*). An increase in the thickness of the formed PEO oxide layer/decrease in the thickness of the unoxidized aluminium layer leads to an increase in the bond strength of the double-layer Al–Al₂O₃ coating with the steel base. At the same time, the maximum adhesion strength of the two-layer coating to the steel base is achieved with a thickness of the unoxidized aluminium layer of 35 μm and is of 61 MPa (Fig. 5, *d*) that corresponds to the value obtained from the results of theoretical calculations of the thickness of the unoxidized aluminium layer from 35 μm to 40 μm .

At such thicknesses of the unoxidized layer of Al on the surface of the steel base, after flashes of instantaneous point sources of heat during PEO, the temperature exceeds 1000 °C, *i.e.*, mutual diffusion processes of Al into the steel base and Fe into the unoxidized layer of aluminium occur, which ensures an increase in the adhesion strength of the coating due to the emergence of a diffusion bond in 1.56 times. In the case of applying PEO to the entire thickness of the Al coating of 250 μm , the bond strength of the obtained oxide coating with the base decreases to 11 MPa (Fig. 5, *e*) due to the occurrence of electrical breakdowns on the steel, which does not have valve properties.

Fig. 7. The wear resistance of the two-layer Al–Al₂O₃ coating with a thickness of 250 μm on a carbon steel 45 substrate with different thickness of the unoxidized Al layer: 125 μm (a); 65 μm (b); 35 μm (c); 0 μm (d)

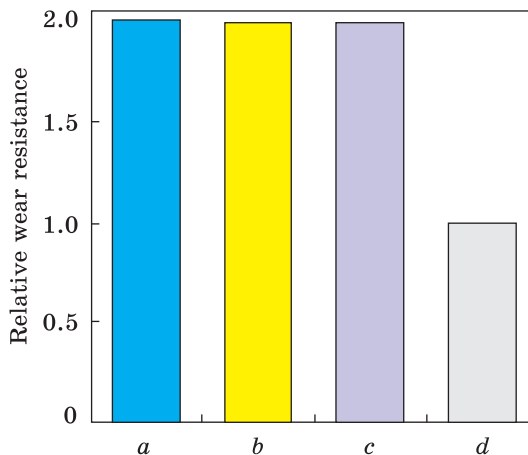


Figure 6 shows the results of testing steel samples with coatings for resistance to sulphide cracking in electrolyte according to Standard TM0177–2005 for 720 hours.

An aluminium coating with a thickness of 250 μm increases the resistance to sulphide cracking of carbon steel 45, the static hydrogen fatigue limit of which is of 0.2 from the yield point (Fig. 6, e) to 0.94 from the yield point (Fig. 6, a). Oxidation of the outer part of the aluminium coating layer significantly increases the resistance of steel to sulphide cracking (Fig. 6, b–d). Thus, the maximum limit of static hydrogen fatigue (1.07) is reached at a thickness of the unoxidized aluminium layer of 65 μm (Fig. 6, c). A further increase in the thickness of the formed PEO oxide layer/decrease in the thickness of the unoxidized aluminium layer leads to a decrease in the static hydrogen fatigue limit of steel with a two-layer coating (Fig. 6, d). The protective effect of two-layer coatings is related to the shielding and electrochemical effect. The significant protective effect of the two-layer Al–Al₂O₃ coating can be explained by the increase in the shielding effect of the oxide layer. Due to the increased volume of aluminium oxide formed during PEO, compared to the volume of aluminium used ($V_{\text{Al}_2\text{O}_3}/V_{\text{Al}} = 1.31$), the closing of pores and the formation of residual compressive stresses in the oxide layer of the coating are ensured. This effect helps to slow down the process of H₂S diffusion from the electrolyte through the layered coating to the steel base, and accordingly, the amount of depolarizer H⁺ decreases, and the catalytic action of hydrogen sulphide on the recombination of hydrogen atoms weakens, which ultimately prevents flooding of the steel and its cracking.

The results of wear tests are presented in Fig. 7.

The analysis of the results shows the high wear resistance of the oxide layer of the two-layer Al–Al₂O₃ coating, comparable to carbon steel 45. It should be noted that the increase in the thickness of the formed PEO oxide layer/decrease in the thickness of the unoxidized aluminium layer practically does not affect the amount of wear of the samples (Fig. 7, a–c).

In general, the test results carried out, according to Figs. 5–7, show, that during the construction of two-layer Al–Al₂O₃ coatings, the thickness of the unoxidized Al layer, which is calculated theoretically and confirmed experimentally, must be chosen from the condition of increasing the adhesion strength of the layered coating to the steel base, and the thickness of the Al₂O₃ oxide layer must be chosen from the condition of ensuring the specified service life of machine parts for wear. In addition, the developed two-layer Al–Al₂O₃ coating also provides effective protection of carbon steel against flooding, embrittlement and cracking in hydrogen sulphide environments. The advantage of proposed two-layered Al–Al₂O₃ coatings with respect to the hard-faced layers [114] is the significantly higher resistance in the hydrogen-enriched environments.

In further research, it is planned to experimentally establish the thickness of the unoxidized aluminium layer adjacent to the steel surface of the two-layer Al–Al₂O₃ coating, the oxide layer of which is formed by PEO, at which diffusion processes begin to occur at the steel base–aluminium interface, as well as study the distribution of chemical elements in this zone and make a comparison with the results of theoretical calculations.

4. Conclusions

As a result of the research, we can summarize and conclude as follows below.

- An analysis of strengthening technologies and the influence of plasma electrolytic oxidation regimes of valve metal materials on the structure, microstructure and physical and mechanical properties of oxide coatings was carried out.

- The technology of forming on steel by the combined method of double-layer Al–Al₂O₃ coatings, using PEO in the electrolyte has been improved; a mathematical model of temperature distribution during PEO of an aluminium coating layer applied to a long cylindrical steel part was constructed.

- The procedure for analytical research of the temperature distribution in a steel cylinder covered with a layer of aluminium at the interface of the components of the two-layer Al–Al₂O₃ coating during PEO was developed.

- It was established that, with a thickness of the unoxidized aluminium layer from 0.035 to 0.040 mm, the temperature on the surface of the steel cylinder after flashes of instantaneous point heat sources from the action of electric-spark discharges during the PEO of the outer part of the aluminium layer exceeds 1000 °C and is more than $0.4T_m$ (here, T_m is a melting temperature of aluminium/steel). Thus, at the

theoretically determined thickness of the unoxidized aluminium layer adjacent to the surface of the steel, mutual diffusion processes will occur at the steel–aluminium interface, that is, the diffusion of iron from steel to aluminium and *vice versa*, from aluminium to steel, which will ensure the emergence of a diffuse connection (welding) of unoxidized layer of aluminium to the steel base of two-layer Al–Al₂O₃ coating: inner—unoxidized layer of aluminium, outer—aluminium oxide layer formed in the PEO process.

The test results shows that in a two-layer Al–Al₂O₃ coating, the thickness of the unoxidized Al layer, which is calculated theoretically and confirmed experimentally, must be chosen from the condition of increasing the adhesion strength of the coating to the steel base due to the emergence of a diffusion bond, and the thickness of the Al₂O₃ oxide layer must be chosen from the condition of ensuring the specified service life of machine parts for wear.

Acknowledgements. The authors are grateful to the Ministry of Science and Education of Ukraine for the grant to implement projects 0122U002082 and 0123U101858. The authors are grateful for thorough consultations of Felix Stotskii and Vasyl Vytvytskyi (Ivano-Frankivsk National Technical University of Oil and Gas) and Mykhailo Student (Karpenko Physico-Mechanical Institute of the National Academy of Sciences of Ukraine). The authors thank the team of the Centre for collective use of scientific instruments ‘Centre for Electron Microscopy and X-Ray Microanalysis’ of the Karpenko Physico-Mechanical Institute of the National Academy of Sciences of Ukraine (Lviv) for promptly conducting microscopic studies of PEO ceramic coatings. The team of authors express their gratitude to the reviewers for valuable recommendations that have been taken into account to improve significantly the quality of this paper.

REFERENCES

1. P. Le Billon and B. Kristoffersen, *Environment and Planning A: Economy and Space*, **52**, No. 6: 1072 (2020);
<https://doi.org/10.1177/0308518X18816702>
2. D. Mara, S. Nate, A. Stavvytsky, and G. Kharlamova, *Energies*, **15**, No. 2: 658 (2022);
<https://doi.org/10.3390/en15020658>
3. *International Energy Agency (IEA), World Energy Outlook. Flagship Report — 2021* (Paris, France: 2021);
<https://www.iea.org/reports/world-energy-outlook-2021>
4. J.-H. Kim and Y.-G. Lee, *Sustainability*, **12**, No. 16: 6628 (2020);
<https://doi.org/10.3390/su12166628>
5. I.I. Chudyk, Ya.M. Femiak, M.I. Orynychak, A.K. Sudakov, and A.I. Riznychuk, *Naukovyi Visnyk Natsionalnoho Hirnychoho Universytetu* **2021**, No. 4: 17 (2021);
<https://doi.org/10.33271/nvngu/2021-4/017>

6. O. Ovetska, S. Ovetskyi, and O. Vytiaz , *E3S Web of Conferences*, **230**: 01021 (2021);
<https://doi.org/10.1051/e3sconf/202123001021>
7. V. Klymenko, S. Ovetskyi, O. Vytyaz, A. Uhrynovskiy, and V. Martynenko, *Mining of Mineral Deposits*, **16**, No. 3: 11 (2022);
<https://doi.org/10.33271/mining16.03.011>
8. O. Bazaluk, A. Velychkovych, L. Ropyak, M. Pashechko, T. Pryhorovska, and V. Lozynskiy, *Energies*, **14**, No. 14: 4198 (2021);
<https://doi.org/10.3390/en14144198>
9. T. Tutko, O. Dubei, L. Ropyak, and V. Vytvytskyi, *Advances in Design, Simulation and Manufacturing IV. DSMIE 2021. Lecture Notes in Mechanical Engineering* (Eds. V. Ivanov, J. Trojanowska, I. Pavlenko, J. Zajac, and D. Peraković) (Cham, Switzerland: Springer: 2021), p. 153;
https://doi.org/10.1007/978-3-030-77719-7_16
10. I. Shatskyi, I. Vytvytskyi, M. Seniushkovych, and A. Velychkovych, *IOP Conf. Series: Materials Science and Engineering*, **564**, 012073 (2019);
<https://doi.org/10.1088/1757-899X/564/1/012073>
11. A. Velychkovych, *Engineering Solid Mechanics*, **2022**, No. 10: 287;
<https://doi.org/10.5267/j.esm.2022.3.002>
12. T. O. Pryhorovska, *Machining Science and Technology*, **21**, No. 1: 37 (2017);
<https://doi.org/10.1080/10910344.2016.1260429>
13. O. Slabyi, *East-Eur. J. Enterp. Technol.*, **3**, No. 7: 27 (2018);
<https://doi.org/10.15587/1729-4061.2018.132661>
14. O. Bazaluk, O. Slabyi, V. Vekeryk, A. Velychkovych, L. Ropyak, and V. Lozynskiy, *Energies*, **14**, No. 12: 3514 (2021);
<https://doi.org/10.3390/en14123514>
15. O. Bazaluk, O. Dubei, L. Ropyak, M. Shovkoplias, T. Pryhorovska, and V. Lozynskiy, *Energies*, **15**, No. 1: 83 (2022);
<https://doi.org/10.3390/en15010083>
16. O.V. Panevnyk and O.Ya. Dubei, *Naukovyi Visnyk Natsionalnoho Hirnychoho Universytetu*, No. 4: 98 (2015).
17. O. Mandryk, V. Artym, M. Shtohry, and V. Zaytsev, *Management Systems in Production Engineering*, **28**, No. 3: 168 (2020);
<https://doi.org/10.2478/mspe-2020-0025>
18. S. Ilin, L. Adorska, V. Samusia, D. Kolosov, and I. Ilina, *E3S Web of Conferences*, **109**: 00030 (2019);
<https://doi.org/10.1051/e3sconf/201910900030>
19. V. Lozynskiy, R. Dychkovskiy, P. Saik, and V. Falshtynskiy, *Solid State Phenomena*, **277**: 66 (2018);
<https://doi.org/10.4028/www.scientific.net/SSP.277.66>
20. M. Petlovanyi, V. Lozynskiy, P. Saik, and K. Sai, *E3S Web of Conferences*, **123**: 01019 (2019);
<https://doi.org/10.1051/e3sconf/201912301019>
21. M. Khoma, V. Vynar, M. Chuchman, and C. Vasyliv, *Lecture Notes in Civil Engineering* **102**: 2311 (2021);
https://doi.org/10.1007/978-3-030-58073-5_18
22. H.M. Nykyforchyn, O.I. Zvirko, and O.T. Tsyruynyk, *Procedia Structural Integrity*, **2**: 501 (2016);
<https://doi.org/10.1016/j.prostr.2016.06.065>
23. M. Khoma, V. Vynar, C. Vasyliv, M. Chuchman, B. Datsko, V. Ivashkiv, and O. Dykha, *Journal of Bio- and Tribo-Corrosion*, **8**: 53 (2022);
<https://doi.org/10.1007/s40735-022-00655-3>

24. O.Y. Andreikiv, I.Y. Dolins'ka, I.P. Shtoiko, O.K. Raiter, and Y.Y. Matviiv, *Materials Science*, **54**: 638 (2019);
<https://doi.org/10.1007/s11003-019-00228-9>
25. M.M. Student, V.M. Dovhunya, V.M. Posuvailo, I.V. Koval'chuk, and V.M. Hvozdet'skyi, *Materials Science*, **53**: 359 (2017);
<https://doi.org/10.1007/s11003-017-0083-x>
26. V. Hutsaylyuk, M. Student, V. Dovhunya, V. Posuvailo, O. Student, P. Maruschak, and I. Koval'chuk, *Metals*, **9**, No. 3: 280 (2019);
<https://doi.org/10.3390/met9030280>
27. K.O. Cooke, *Aluminium Alloys and Composites* (Ed. K.O. Cooke) (London, United Kingdom: IntechOpen: 2020), p. 1;
<https://doi.org/10.5772/intechopen.90569>
28. V.I. Pokhmurskii, I.M. Zin, V.A. Vynar, O.P. Khlopyk, and L.M. Bily, *Corrosion Engineering Science and Technology*, **47**, No. 3: 182 (2012);
<https://doi.org/10.1179/1743278211Y.0000000022>
29. K. Berladir, T. Hovorun, O. Gusak, Y. Reshetniak, and D. Khudaybergenov, *Advances in Design, Simulation and Manufacturing III. DSMIE 2020. Lecture Notes in Mechanical Engineering* (Eds. V. Ivanov, J. Trojanowska, I. Pavlenko, J. Zajac, and D. Peraković) (Cham, Switzerland: Springer: 2020) p. 473;
https://doi.org/10.1007/978-3-030-50794-7_46
30. C.-H. Hsu, *Metals*, **10**, No. 5: 605 (2020);
<https://doi.org/10.3390/met10050605>
31. M.C. Santos, A.R. Machado, and W.F. Sales, *Int. J. Adv. Manuf. Technol.*, **86**: 3067 (2016);
<https://doi.org/10.1007/s00170-016-8431-9>
32. O. Vlasij, V. Mazurenko, L. Ropyak, and O. Rogal, *East-Eur. J. Enterp. Technol.*, **1**, No. 7 (85): 25 (2017) (in Ukrainian);
<https://doi.org/10.15587/1729-4061.2017.65718>
33. V.I. Pokhmurskii, I.M. Zin, V.A. Vynar, O.P. Khlopyk, and L.M. Bily, *Corrosion Engineering Science and Technology* **47**, No. 3: 182;
<https://doi.org/10.1179/1743278211Y.0000000022>
34. M. Sathish, N. Radhika, and B. Saleh, *Composites. Part B: Engineering*, **225**: 109278 (2021);
<https://doi.org/10.1016/j.compositesb.2021.109278>
35. J. Kusyj and A. Kuk, *East-Eur. J. Enterp. Technol.*, **1**, No. 7: 41 (2015);
<https://doi.org/10.15587/1729-4061.2015.36336>
36. V.I. Kyryliv, V.I. Gurey, O.V. Maksymiv, I.V. Hurey, and Y.O. Kulyk, *Materials Science*, **57**: 422 (2021);
<https://doi.org/10.1007/s11003-021-00556-9>
37. B.N. Mordyuk, V.V. Silberschmidt, G.I. Prokopenko, Y.V. Nesterenko, and M.O. Iefimov, *Materials Characterization*, **61**, No. 11: 1126 (2010);
<https://doi.org/10.1016/j.matchar.2010.07.007>
38. H.V. Pokhmurs'ka, M.M. Student, N.R. Chervins'ka, Kh.R. Smetana, A. Wank, T. Hoenig, and H. Podlesak, *Materials Science*, **41**: 316 (2005);
<https://doi.org/10.1007/s11003-005-0168-9>
39. M.M. Student, I.M. Pohrelyuk, V.M. Hvozdet'skyi, H.H. Veselivska, K.R. Zadorozhna, R.S. Mardarevych, and Y.V. Dzioba, *Materials Science*, **57**: 240 (2021);
<https://doi.org/10.1007/s11003-021-00538-x>
40. F. Peltier and D. Thierry, *Coatings*, **12**: 518 (2022);
<https://doi.org/10.3390/coatings12040518>

41. O. Gaponova, C. Kundera, G. Kirik, and V. Tarelnyk, V. Martsynkovskyy, I. Konoplianchenko, M. Dovzhyk, A. Belous, and O. Vasilenko, *Advances in Thin Films, Nanostructured Materials, and Coatings. Lecture Notes in Mechanical Engineering* (Eds. A. Pogrebnjak and V. Novosad) (Singapore: Springer: 2019), p. 249;
https://doi.org/10.1007/978-981-13-6133-3_25
42. S.I. Kryshchtopa, D.Yu. Petryna, I.M. Bogatchuk, I.B. Prun'ko, and V.M. Mel'nyk, *Alloying Mater. Sci.*, **53**, No. 3: 351 (2017);
<https://doi.org/10.1007/s11003-017-0082-y>
43. Z.A. Duryagina, S.A. Bespalov, V.Ya. Pidkova, and D.Yu. Polockyj, *Metallofiz. Noveishie Tekhnol.*, **33**, Spec. Iss.: 393 (2011).
44. V. Hutsaylyuk, M. Student, K. Zadorozhna, O. Student, H. Veselivska, V. Gvosdetskii, P. Maruschak, and H. Pokhmurska, *J. Mater. Res. Technol.*, **9**, No. 6: 16367 (2020);
<https://doi.org/10.1016/j.jmrt.2020.11.102>
45. T.W. Clyne and S.C. Troughton, *Int. Mater. Rev.*, **64**, No. 3: 127 (2019);
<https://doi.org/10.1080/09506608.2018.1466492>
46. F. Simchen, M. Sieber, A. Kopp, and T. Lampke, *Coatings*, **10**, No. 7: 628 (2020);
<https://doi.org/10.3390/coatings10070628>
47. S. Sikdar, P.V. Menezes, R. Maccione, T. Jacob, and P.L. Menezes, *Nanomaterials* **11**, No. 6: 1375 (2021);
<https://doi.org/10.3390/nano11061375>
48. M. Kaseem and B. Dikici, *Coatings*, **11**, No. 6: 374 (2021);
<https://doi.org/10.3390/coatings11040374>
49. L. Ropyak, T. Shihab, A. Velychkovych, V. Bilinskyi, V. Malinin, and M. Romaniv, *Ceramics*, **6**, No. 1: 146 (2023);
<https://doi.org/10.3390/ceramics6010010>
50. M.M. Student and I.M. Pohrelyuk, *Mater. Sci.*, **57**: 377 (2021);
<https://doi.org/10.1007/s11003-021-00552-z>
51. Q. Tang, T. Qiu, P. Ni, D. Zhai, and J. Shen, *Coatings*, **12**, No. 8: 1191 (2022);
<https://doi.org/10.3390/coatings12081191>
52. V.A. Andrei, C. Radulescu, V. Malinovschi, A. Marin, E. Coaca, M. Mihalache, C.N. Mihailescu, I.D. Dulama, S. Teodorescu, and I.A. Bucurica, *Coatings*, **10**, No. 4: 318 (2020);
<https://doi.org/10.3390/coatings10040318>
53. N. Attarzadeh, M. Molaei, K. Babaei, and A. Fattah-Alhosseini, *Surf. Interfaces*, **23**: 100997 (2021);
<https://doi.org/10.1016/j.surf.2021.100997>
54. X. Nie, R. Cai, C. Zhao, J. Sun, J. Zhang, and D.T.A. Matthews, *Surf. Coat. Technol.*, **442**: 128403 (2022);
<https://doi.org/10.1016/j.surfcoat.2022.128403>
55. L. Ropyak and V. Ostapovych, *East-Eur. J. Enterp. Technol.*, **2**, No. 5: 50 (2016);
<https://doi.org/10.15587/1729-4061.2016.65719>
56. V.S. Protsenko, L.S. Bobrova, A.S. Baskevich, S.A. Korniy, and F.I. Danilov, *J. Chem. Technol. Metallurgy*, **53**: 906 (2018).
57. V.S. Protsenko, L.S. Bobrova, D.E. Golubtsov, S.A. Korniy, and F.I. Danilov, *Russ. J. Applied Chemistry* **91**: 1106 (2018);
<https://doi.org/10.1134/S1070427218070066>
58. O.Y. Dubei, T.F. Tutko, L.Y. Ropyak, and M.V. Shovkoplias, *Metallofiz. Noveishie Tekhnologii*, **44**, No. 5: 251 (2022);
<https://doi.org/10.15407/mfint.44.02.0251>

59. M. Dutkiewicz, A. Velychkovych, I. Shatskyi, and V. Shopa, *Materials*, **15**, No. 13: 4671 (2022);
<https://doi.org/10.3390/ma15134671>
60. K. Ye and Z. Li, *Corrosion*, **76**, No. 10: 895 (2020);
<https://doi.org/10.5006/3560>
61. P. Hartjen, A. Hoffmann, A. Henningsen, M. Barbeck, A. Kopp, L. Kluwe, C. Precht, O. Quatela, R. Gaudin, M. Heiland, R.E. Friedrich, C. Knipfer, D. Grubeanu, R. Smeets, and O. Jung, *In Vivo (Athens, Greece)*, **32**, No. 2: 241 (2018).
<https://doi.org/10.21873/invivo.11230>
62. A. Chuzhak, V. Sulyma, L. Ropyak, A. Velychkovych, and V. Vytvytskyi, *J. Healthc. Eng.*, **2021**: 6607364 (2021);
<https://doi.org/10.1155/2021/6607364>
63. O. Bazaluk, A. Chuzhak, V. Sulyma, A. Velychkovych, L. Ropyak, V. Vytvytskyi, V. Mykhailiuk, and V. Lozynskiy, *Appl. Sci.*, **12**, No. 10: 4903 (2022);
<https://doi.org/10.3390/app12104903>
64. S. Dobrotvorskiy, M. Balog, Y. Basova, L. Dobrovolska, and A. Zinchenko, *Advanced Manufacturing Processes. InterPartner 2019. Lecture Notes in Mechanical Engineering* (Eds. V. Tonkonogyi, V. Ivanov, J. Trojanowska, G. Oborskyi, M. Edl, I. Kuric, I. Pavlenko, and P. Dasic) (Cham, Switzerland: Springer: 2020), p. 32;
https://doi.org/10.1007/978-3-030-40724-7_4
65. L.S. Saakiyan, A.P. Efremov, L.Ya. Ropyak, and A.V. Gorbatskii, *Soviet Mater. Sci.*, **23**, No. 3: 267 (1987);
<https://doi.org/10.1007/BF00720884>
66. L.S. Saakiyan, A.P. Efremov, and L. Ya. Ropyak, *Protection of Metals*, **25**, No. 2: 185 (1989).
67. V.A. Vynar, V.I. Pokhmurs'kyi, I.M. Zin', K.B. Vasylyv, and O.P. Khlopyk, *Mater. Sci.*, **53**: 717 (2018);
<https://doi.org/10.1007/s11003-018-0128-9>
68. A. Gulyarenko and M. Bembenek, *Agriculture (Switzerland)*, **12**, No. 6: 841 (2022);
<https://doi.org/10.3390/agriculture12060841>
69. S.I. Kryshchtopa, I.B. Prun'ko, B.V. Dolishnii, M.V. Panchuk, I.M. Bogatchuk, and V.M. Mel'nyk, *Mater. Sci.*, **55**: 187 (2019);
<https://doi.org/10.1007/s11003-019-00288-x>
70. J. Pawlik, A. Wryblewska-Pawlik, and M. Bembenek, *Materials*, **15**, No. 16: 5783 (2022);
<https://doi.org/10.3390/ma15165783>
71. X. Qi, H. Shang, B. Ma, R. Zhang, L. Guo, and B. Su, *Materials*, **13**, No. 4: 970 (2020);
<https://doi.org/10.3390/ma13040970>
72. J.M. Wheeler, J.A. Curran, and S. Shrestha, *Surf. Coat. Technol.* **207**: 480 (2012);
<https://doi.org/10.1016/j.surfcoat.2012.07.056>
73. M.M. Student, V.V. Shmyrko, M.D. Klapkiv, I.M. Lyasota, and L.N. Dobrovol'ska, *Mater. Sci.*, **50**: 290 (2014);
<https://doi.org/10.1007/s11003-014-9720-9>
74. J. Dean, T. Gu, and T.W. Clyne, *Surface and Coatings Technology*, **269**: 47 (2015);
<https://doi.org/10.1016/j.surfcoat.2014.11.006>

75. Z.-Q. Wu, Y. Xia, G. Li, and F.-T. Xu, *Dalian Ligong Daxue Xuebao/Journal of Dalian University of Technology*, **46**: 60 (2006).
76. B.A. Lyashenko, V.S. Veremchuk, N.A. Dolgov, and V.M. Ivanov, *Strength of Materials*, **28**: 452 (1996);
<https://doi.org/10.1007/BF02209316>
77. L.Y. Ropyak, A.S. Velychkovych, V.S. Vytvytskyi, and M.V. Shovkoplias, *J. Phys. Conf. Ser.*, **1741**: 012039 (2021);
<https://doi.org/10.1088/1742-6596/1741/1/012039>
78. R. Tatsiy, M. Stasiuk, O. Pazen, and S. Vovk, *Proceedings of the 2018 International Scientific-Practical Conference on Problems of Infocommunications Science and Technology (Kharkiv, Ukraine: 2018)*, p. 21;
<https://doi.org/10.1109/INFOCOMMST.2018.8632131>
79. M. Bembenek, A. Uhryński, *Materials*, **14**, No. 7: 1770 (2021);
<https://doi.org/10.3390/ma14071770>
80. R.M. Tatsiy, O.Y. Pazen, S.Y. Vovk, and D.V. Kharyshyn, *Naukovyi Visnyk Natsionalnoho Hirnychoho Universytetu*, **3**: 27 (2020);
<https://doi.org/10.33271/nvngu/2020-3/027>
81. J. Pawlik, J. Ciešlik, M. Bembenek, T. Gyrál, S. Kapayeva, and M. Kapkenova, *Materials*, **15**, No. 17: 6019 (2022);
<https://doi.org/10.3390/ma15176019>
82. I. P. Shatskyi, L. Ya. Ropyak, and M. V. Makoviichuk, *Strength of Materials*, **48**, No. 5: 726 (2016);
<https://doi.org/10.1007/s11223-016-9817-5>
83. L.Ya. Ropyak, I.P. Shatskyi, and M.V. Makoviichuk, *Metallofiz. Noveishie Tekhnol.*, **39**, No. 4: 517 (2017);
<https://doi.org/10.15407/mfint.39.04.0517>
84. L.Y. Ropyak, M.V. Makoviichuk, I.P. Shatskyi, I.M. Pritula, L.O. Gryn, and V.O. Belyakovskiy, *Functional Mater.*, **27**, No. 3: 638 (2020);
<https://doi.org/10.15407/fm27.03.638>
85. M. Bembenek, M. Makoviichuk, I. Shatskyi, L. Ropyak, I. Pritula, L. Gryn, and V. Belyakovskiy, *Sensors*, **22**, No. 21: 8105 (2022);
<https://doi.org/10.3390/s22218105>
86. I.P. Shatskyi, M.V. Makoviichuk, and A.B. Shcherbii, *Proc. 11th Int. Conf. Shell Structures: Theory and Applications (SSTA 2017)*, **4**: 165 (2018);
<https://doi.org/10.1201/9781315166605-34>
87. I.P. Shats'kyi, M.V. Makoviichuk, and A.B. Shcherbii, *J. Math. Sci.*, **238**, No. 2: 165 (2019);
<https://doi.org/10.1007/s10958-019-04226-9>
88. I.P. Shatskyi, M.V. Makoviichuk, and A.B. Shcherbii, *Mater. Sci.*, **55**: 484 (2020);
<https://doi.org/10.1007/s11003-020-00329-w>
89. A.A. Bedzir, I.P. Shatskii, and V.M. Shopa, *Int. Appl. Mech.*, **31**, No. 5: 351 (1995);
<https://doi.org/10.1007/BF00846842>
90. I.P. Shats'kyi, O.M. Lyskanych, and V.A. Kornuta, *Strength Mater.*, **48**, No. 3: 469 (2016);
<https://doi.org/10.1007/s11223-016-9786-8>
91. I.P. Shats'kyi, V.M. Shopa, and A.S. Velychkovych, *Strength Mater.*, **53**: 277 (2021); <https://doi.org/10.1007/s11223-021-00286-y>
92. R.M. Tatsiy, O.Y. Pazen, S.Y. Vovk, L.Y. Ropyak, and T.O. Pryhorovska, *J. Serb. Soc. Comput. Mech.*, **13**, No. 2: 36 (2019);
<https://doi.org/10.24874/JSSCM.2019.13.02.04>

93. R.M. Tatsii, M.F. Stasyuk, and O.Y. Pazen, *J. Eng. Phys. Thermophys.*, **94**: 298 (2021); <https://doi.org/10.1007/s10891-021-02302-z>
94. R.M. Tatsii, O.Yu. Pazen, and S.Ya. Vovk, *Naukovyi Visnyk Natsionalnoho Hirnychoho Universytetu*, **2020**, No. 1: 36 (2020); <https://doi.org/10.33271/nvngu/2020-1/036>
95. V.S. Kolesov, N.V. Vlasov, L.O. Tisovskii, and I.P. Shatskii, *Int. Appl. Mech.*, **28**: 426 (1992); <https://doi.org/10.1007/BF00847125>
96. N.I. Malanchuk, B.S. Slobodyan, and R.M. Martynyak, *Materials Science*, **52**: 819 (2017); <https://doi.org/10.1007/s11003-017-0026-6>
97. Y. Kusyi, O. Onysko, A. Kuk, B. Solohub, and V. Kopei, *Lecture Notes in Networks and Systems*, **472**: 135 (2022); https://doi.org/10.1007/978-3-031-05230-9_16
98. T. Pryhorovska and L. Ropyak, *Proc. Int. Conf. on Advanced Optoelectronics and Lasers (CAOL) (Sozopol, Bulgaria, 2019)*, p. 493; <https://doi.org/10.1109/CAOL46282.2019.9019544>
99. L. Ropyak, V. Vytvytskyi, A. Velychkovych, T. Pryhorovska, and M. Shovkoplias, *IOP Conf. Ser.: Mater. Sci. Eng.*, **1018**: 012014 (2021); <http://doi.org/10.1088/1757-899X/1018/1/012014>
100. Y. Kusyi, V. Stupnytskyy, O. Onysko, E. Dragalcius, S. Baskutis, and R. Chatys, *Eksploatacja i Niezawodnosc*, **24**: 655 (2022); <https://doi.org/10.17531/ein.2022.4.684>
101. Y.M. Kusyi and A.M. Kuk, *J. Phys. Conf. Ser.*, **1426**: 012034 (2020); <https://doi.org/10.1088/1742-6596/1426/1/012034>
102. W. Dai, C. Li, D. He, D. Jia, Y. Zhang, and Z. Tan, *Surf. Coat. Technol.*, **380**: 125014 (2019); <https://doi.org/10.1016/j.surfcoat.2019.125014>
103. F. Xi, Y. Huang, Y. Zhao, Y. Liu, W. Dai, and Y. Tian, *Materials*, **15**, No. 12: 4256 (2022); <https://doi.org/10.3390/ma15124256>
104. E. Matykina, R. Arrabal, A. Pardo, M. Mohedano, B. Mingo, I. Rodríguez, and J. González, *Mater. Lett.*, **127**: 13 (2014); <https://doi.org/10.1016/j.matlet.2014.04.077>
105. M. Vakili-Azghandi, A. Fattah-Alhosseini, and M. K. Keshavarz, *Measurement*, **124**: 252259 (2018); <https://doi.org/10.1016/j.measurement.2018.04.038>
106. L. An, Y. Ma, X. Yan, S. Wang, and Z. Wang, *Transactions of Nonferrous Metals Society of China*, **30**, No. 4: 883 (2020); [https://doi.org/10.1016/S1003-6326\(20\)65262-1](https://doi.org/10.1016/S1003-6326(20)65262-1)
107. F. Songur, E. Arslan, and B. Dikici, *Surf. Coat. Technol.*, **434**: 128202 (2022); <https://doi.org/10.1016/j.surfcoat.2022.128202>
108. M.M. Student, I.B. Ivasenko, V.M. Posuvailo, H.H. Veselivs'ka, A.Y. Pokhmurs'kyi, Y.Y. Sirak, and V.M. Yus'kiv, *Mater. Sci.*, **54**: 899 (2019); <https://doi.org/10.1007/s11003-019-00278-z>
109. M. Bembenek, T. Mandziy, I. Ivasenko, O. Berehulyak, R. Vorobel, Z. Slobodyan, and L. Ropyak, *Sensors*, **22**, No. 19: 7600 (2022); <https://doi.org/10.3390/s22197600>
110. I. Ivasenko, V. Posuvailo, H. Veselivska, and V. Vynar, *Int. Sci. Tech. Conf. Comp. Sci. Inform. Technol.*, **2**, 9321900: 50 (2020); <https://doi.org/10.1109/CSIT49958.2020.9321900>

111. V.B. Kopei, O.R. Onysko, and V.G. Panchuk, *J. Phys. Conf. Ser.*, **1426**, No. 1: 012033 (2020);
<https://doi.org/10.1088/1742-6596/1426/1/012033>
112. Y.M. Kusyi and A.M. Kuk, *J. Phys. Conf. Ser.*, **1426**: 012034 (2020);
<https://doi.org/10.1088/1742-6596/1426/1/012034>
113. M. Kaseem, S. Fatimah, N. Nashrah, Y.G. Ko, *Progress in Materials Science*, **117**: 100735 (2021);
<https://doi.org/10.1016/j.pmatsci.2020.100735>
114. M. Bembenek, P. Prysyazhnyuk, T. Shihab, R. Machnik, O. Ivanov, and L. Ropyak, *Materials*, **15**, No.14: 5074 (2022);
<https://doi.org/10.3390/ma15145074>
115. I.M. Melnyk, T.M. Radchenko, and V.A. Tatarenko, *Metallofiz. Noveishie Tekhnol.*, **32**, No. 9: 1191 (2010) (in Ukrainian).
116. T.M. Radchenko, O.S. Gatsenko, V.V. Lizunov, and V.A. Tatarenko, *Prog. Phys. Met.*, **21**, No. 4: 580 (2020);
<https://doi.org/10.15407/ufm.21.04.580>
117. T. Shihab, P. Prysyazhnyuk, I. Semyanyk, R. Anrusyshyn, O. Ivanov, L. Troshchuk, *Manag. Syst. Prod. Eng.*, **28**, No. 2: 84 (2020);
<https://doi.org/10.2478/mspe-2020-0013>
118. A.G. Solomenko, R.M. Balabai, T.M. Radchenko, and V.A. Tatarenko, *Prog. Phys. Met.*, **23**, No. 2: 147 (2022);
<https://doi.org/10.15407/ufm.23.02.147>
119. P. Prysyazhnyuk, L. Shlapak, I. Semyanyk, V. Kotsyubynsky, L. Troshchuk, S. Korniy, and V. Artym, *East-Eur. J. Enterp. Technol.*, **6**, No. 12: 28 (2020);
<https://doi.org/10.15587/1729-4061.2020.217281>
120. V. Pokhmurskii, H. Nykyforchyn, M. Student, M. Klapkiv, H. Pokhmurska, B. Wielage, T. Grund, A. Wank, *Proc. Int. Thermal Spray Conf.*, **16**: 998 (2007);
<https://doi.org/10.1007/s11666-007-9104-x>
121. M.M. Student, V.M. Posuvailo, H.H. Veselivs'ka, Y.Y. Sirak, and R.A. Yatsyuk, *Mater. Sci.*, **53**: 789 (2018);
<https://doi.org/10.1007/s11003-018-0137-8>
122. M. Shao, W. Wang, H. Yang, X. Zhang, and X. He, *Coatings*, **11**, No. 11: 1288 (2021);
<https://doi.org/10.3390/coatings11111288>
123. A.H. Pakseresht, M. Saremi, H. Omidvar, and M. Alizadeh, *Surf. Coat. Technol.*, **366**: 338 (2019);
<https://doi.org/10.1016/j.surfcoat.2019.03.059>
124. A.M. Kamalan Kirubaharan and P. Kuppasami, *Micro and Nano Technologies. Corrosion Protection at the Nanoscale* (Ed. S. Rajendran) (Amsterdam: Elsevier: 2020), p. 295;
<https://doi.org/10.1016/B978-0-12-819359-4.00016-7>
125. V. Hutsaylyuk, M. Student, V. Posuvailo, O. Student, Y. Sirak, V. Hvozdets'kyi, P. Maruschak, and H. Veselivska, *Vacuum*, **179**: 109514 (2020);
<https://doi.org/10.1016/j.vacuum.2020.109514>
126. B.-J. Wei, Y.-L. Cheng, Y.-Y. Liu, Z.-D. Zhu, and Y.-L. Cheng, *Transactions of Nonferrous Metals Society of China*, **31**, 2287 (2021);
[https://doi.org/10.1016/S1003-6326\(21\)65655-8](https://doi.org/10.1016/S1003-6326(21)65655-8)
127. H. Berekatain and S.M. Mousavi Khoei, *Surf. Coat. Technol.*, **384**: 125339 (2020);
<https://doi.org/10.1016/j.surfcoat.2020.125339>
128. J. Zhang, Y. Fan, X. Zhao, R. Ma, A. Du, and X. Cao, *Surf. Coat. Technol.*, **337**: 141 (2018); <https://doi.org/10.1016/j.surfcoat.2017.12.064>

129. A. Lypez-Ortega, J.L. Arana, E. Rodríguez, and R. Bayyn, *Corrosion Sci.*, **143**: 258 (2018);
<https://doi.org/10.1016/j.corsci.2018.08.001>
130. L. Lu, D. Shen, J. Zhang, and C. Guo, *Applied Mechanics and Materials*, **152–154**: 40 (2012);
<https://doi.org/10.4028/www.scientific.net/AMM.152-154.40>
131. L. Lu, J. Zhang, D. Shen, L. Wu, G. Jiang, and L. Li, *J. Alloys Compd.*, **512**: 57 (2012);
<https://doi.org/10.1016/j.jallcom.2011.08.103>
132. J.H. Zhao, G.H. Zhao, T. Li, X. Liu, J.L. Li, and E. Han, Structure and properties of composite ceramic coatings on H13 steel by hot dipping aluminium and plasma electrolytic oxidation. *Cailiao Rechuli Xuebao/Trans Mater. Heat Treat.*, **33**: 129 (2012).
133. W.C. Gu, G.H. Lv, H. Chen, G.L. Chen, W.R. Feng, G.L. Zhang, and S.Z. Yang, *J. Alloys Compd.*, **430**: 308 (2007);
<https://doi.org/10.1016/j.jallcom.2006.05.030>
134. Z. Wu, Y. Xia, G. Li, and F. Xu, *Appl. Surf. Sci.*, **253**: 8398 (2007);
<https://doi.org/10.1016/j.apsusc.2007.04.007>
135. W.C. Gu, D.J. Shen, Y.L. Wang, G.L. Chen, W.R. Feng, G.L. Zhang, S.H. Fan, C.Z. Liu, and S.Z. Yang, *Appl. Surf. Sci.*, **252**, No. 8: 2927 (2006);
<https://doi.org/10.1016/j.apsusc.2005.04.036>
136. B. Wielage, D. Meyer, H. Pokhmurska, G. Alisch, and T. Grund, *Materialwissenschaft und Werkstofftechnik*, **39**: 920 (2008);
<https://doi.org/10.1002/mawe.200800407>
137. T. Lampke, D. Meyer, G. Alisch, D. Nickel, I. Scharf, L. Wagner, and U. Raab, *Surf. Coat. Technol.*, **206**, No. 7: 2012 (2011);
<https://doi.org/10.1016/j.surfcoat.2011.09.006>
138. T. Lampke, D. Meyer, G. Alisch, B. Wielage, H. Pokhmurska, M. Klapkiv, and M. Student, *Materials Science*, **46**: 591 (2011);
<https://doi.org/10.1007/s11003-011-9328-2>
139. S. Durdu, S. L. Aktuğ, and K. Korkmaz, *Surf. Coat. Technol.*, **236**: 303 (2013);
<https://doi.org/10.1016/j.surfcoat.2013.10.004>
140. Z. Chen, K. Zhou, X. Lu, and Y. Lam, *Acta Mechanica*, **225**: 431 (2014);
<https://doi.org/10.1007/s00707-013-0979-y>
141. B.N.J. Persson and M. Scaraggi, *J. Chem. Phys.*, **141**, No. 12: 124701 (2014);
<https://doi.org/10.1063/1.4895789>
142. G. Abadias, E. Chason, J. Keckes, M. Sebastiani, G.B. Thompson, E. Barthel, G.L. Doll, C.E. Murray, C.H. Stoessel, and L. Martinu, *J. Vacuum Sci. Technol. A*, **36**, No. 2: 020801 (2018);
<https://doi.org/10.1116/1.5011790>
143. Ya.S. Pidstryhach, V.A. Lomakin, and Yu.M. Koliano, *Thermoelasticity of Bodies of Inhomogeneous Structure* (Moskva: Nauka: 1984) (in Russian).
144. M. Dutkiewicz, T. Dalyak, I. Shatskyi, T. Venhrynyuk, and A. Velychkovych, *Appl. Sci.*, **11**, No. 22: 10676 (2021);
<https://doi.org/10.3390/app112210676>
145. J. Yang, *Theory of Thermal Conductivity* (Boston: Springer: 2004);
https://doi.org/10.1007/0-387-26017-X_1
146. E.M. Kartashov, *Analytical Methods in the Theory of Thermal Conductivity of Solids* (Moskva: Vysshaya Shkola: 1985) (in Russian).
147. A.I. Lurie, *Theory of Elasticity* (Berlin: Springer: 2010)

148. Ya.S. Pidstryhach, Yu.A. Chernukha, and N.I. Voitovich, *Doklady AN UkrSSR, Ser. A*, **5**: 429 (1975).
149. Ya.S. Pidstryhach, N.I. Voitovich, and Yu.A. Chernukha, *Mathematical Methods and Physical-Mechanical Fields*, **3**: 15 (1976)
150. Y.S. Podstrigach, Y.A. Chernykha, and N.I. Voitovich, *Strength of Materials*, **18**: 686 (1986);
<https://doi.org/10.1007/BF01522787>
151. B.A. Boley and J.H. Weiner, *Theory of Thermal Stresses* (New York: Dover Publications: 2012).
152. A. Bandura and O. Skaskiv, *Rocky Mountain J. Math.*, **49**, No. 4: 1063 (2019);
<https://doi.org/10.1216/RMJ-2019-49-4-1063>
153. A. Bandura and O. Skaskiv, *Demonstration Math.*, **52**, No. 1: 82 (2019);
<https://doi.org/10.1515/dema-2019-0008>
154. O. Posiko and M. Sheremeta, *Integral Transforms Spec. Funct.*, **18**, No. 4: 271 (2007);
<https://doi.org/10.1080/10652460600935387>
155. M.M. Sheremeta and A.O. Kuryliak, *Mat. Stud.*, **50**, No. 1: 22 (2018);
<https://doi.org/10.15330/ms.50.1.22-35>
156. H. Grauert, *The Methods of the Theory of Functions of Several Complex Variables* (Berlin–Heidelberg: Springer: 1991);
https://doi.org/10.1007/978-3-642-76709-8_8
157. B. Lépson, *Proc. Sympos. Pure Math.* **11**: 298 (1968).
158. V. Baksa, A. Bandura, and O. Skaskiv, *Constr. Math. Anal.*, **3**, No. 1: 9 (2020);
<https://doi.org/10.33205/CMA.650977>
159. M. German and P. Grinchuk, *J. Eng. Phys. Thermophys.*, **75**: 1301 (2002);
<https://doi.org/10.1023/A:1022150523156>
160. A.F. Chudnovsky, *Thermophysical Characteristics of Dispersed Materials* (Moskva: Fizmatgiz: 1962) (in Russian).
161. P. Jadhav, A. Bongale, S. Kumar, D.Y. Pimenov, K. Giasin, and S. Wojciechowski, *Materials*, **15**, No. 4: 1616 (2022);
<https://doi.org/10.3390/ma15041616>
162. I.S. Gradshteyn and I.M. Ryzhik, *Tables of Integrals, Series and Products* (Elsevier: 2014);
<https://doi.org/10.1016/C2010-0-64839-5>
163. A.H. Chokshi and M.A. Meyers, *Scr. Metall. Mater.*, **24**, No. 4: 605 (1990);
[https://doi.org/10.1016/0956-716X\(90\)90209-Y](https://doi.org/10.1016/0956-716X(90)90209-Y)
164. A.V. Sergueeva, N.A. Mara, and A.K. Mukherjee, *MRS Online Proceedings Library*, **821**: 336 (2004);
<https://doi.org/10.1557/PROC-821-P9.8>
165. A.A. Shirzadi, C. Zhang, M.Z. Mughal, and P. Xia, *Metals*, **12**, No. 7: 1193 (2022);
<https://doi.org/10.3390/met12071193>

Received 06.04.2023;
in final version, 06.06.2023

Л. Роп'як¹, Т. Шіхаб^{2,1}, А. Величкович¹,
О. Дубей¹, Т. Тутко¹, В. Білінський¹

¹ Івано-Франківський національний технічний університет нафти і газу,
вул. Карпатська, 15, 76019 Івано-Франківськ, Україна

² Інженерно-технічний коледж, Університет Аль-Баян,
Дорога міжнародного аеропорту, поряд з площею Аббаса бін Фірнас,
10070 Багдад–Джадрія, Ірак

РОЗРОБКА ДВОШАРОВОГО ПОКРИТТЯ Al–Al₂O₃ З ОКСИДНИМ ШАРОМ, СФОРМОВАНИМ ПЛАЗМОВИМ ЕЛЕКТРОЛІТИЧНИМ ОКСИДУВАННЯМ АЛЮМІНІЮ, ДЛЯ ЗАХИСТІВ КРИЦІ ВІД КОРОЗІЇ ТА ЗНОШУВАННЯ

Проаналізовано технології формування покриттів для захисту деталей машин і обладнання від корозії та зношування в агресивних середовищах. Розглядається вплив режимів плазмового електролітичного оксидування (ПЕО) вентильних металічних матеріалів на будову, мікроструктуру та фізико-механічні властивості оксидних покриттів. Для вирішення цієї проблеми перспективною є розробка комбінованої технології: нанесення шару алюмінію на поверхню крицевих деталей з подальшим його ПЕО. Метою даної роботи є теоретичне дослідження розподілу температури у крицевому циліндрі, покритому шаром алюмінію, під час ПЕО для обґрунтування товщини шарів двошарового покриття алюміній–оксид алюмінію. Розроблено установку для ПЕО та технологічний процес формування двошарового покриття Al–Al₂O₃ на довгомірних деталях. Створено математичну модель нескінченного тришарового циліндра з внутрішнім коаксіальним поверхневим циліндричним джерелом тепла, що рухається з постійною швидкістю в радіальному напрямку вглиб алюмінійового шару циліндра. Модель засновано на розв'язанні крайової задачі теплопровідності з умовою ідеального теплового контакту між шарами. Під час ПЕО утворюється твердий оксидний шар, але товщина непрооксидованого шару алюмінію зменшується. Теплофізичні характеристики такого циліндра є функціями радіальної координати циліндра та часу. Під час побудови двошарового покриття доцільно використовувати результати теплових розрахунків для обґрунтування товщини прилеглого до поверхні криці шару неоксидованого алюмінію за умови забезпечення перебігу процесів взаємної дифузії на межі поділу між алюмінієм і крицею для підвищення міцності зчеплення покриття з основою за рахунок нагрівання миттєвими джерелами тепла, спричинених дією іскрових електричних розрядів у процесі ПЕО. Товщина зовнішнього суцільного шару оксиду алюмінію вибирається з умови забезпечення необхідного терміну служби деталей машин на зношування з певним збереженням. Результати проведених механічних, трибологічних випробувань і випробування на корозійне розтріскування крицевих зразків з розробленим двошаровим покриттям Al–Al₂O₃ показали високі його експлуатаційні властивості.

Ключові слова: двошарове покриття, алюміній, оксид алюмінію, криця, математична модель, температура, дифузія.